Joint Transceiver Design for Dual-Functional Full-Duplex Relay Aided Radar-Communication Systems

Yinghui He, *Student Member, IEEE,* Yunlong Cai, *Senior Member, IEEE,* Guanding Yu, *Senior Member, IEEE,* and Kai-Kit Wong, *Fellow, IEEE*

Abstract—Driven by the demand for massive and accurate sensing data to achieve wireless network intelligence under a limited available spectrum, the coexistence between radar and communication systems has attracted public attention. In this paper, we investigate a novel dual-functional full-duplex relay aided radar-communication system where the phased-array radar is employed at the amplify-and-forward (AF) relay. A joint transceiver design is proposed to maximize the minimum signal-to-interference-plus-noise ratio (SINR) among all detection directions at the radar receiver under communication quality-of-service and total energy constraints. The formulated optimization problem is particularly challenging due to the highly nonconvex objective function and constraints. Based on the problem structure, we equivalently decompose it into the radar-energy and relay-energy minimization problems under SINR requirements. To solve the radar-energy minimization problem, we propose a low-complexity algorithm based on the alternating direction method of multipliers to optimize the radar transmit power and receiver. The relay-energy minimization problem can be simplified into an equivalent quadratic programming problem by introducing an insightful unitary matrix. Then, the closed-form expression for the AF relay beamforming matrix can be derived, which is jointly determined by the channel condition of relay communication and the detection direction of the radar. After that, we introduce the overall transceiver design algorithm to the original problem and discuss its optimality and computational complexity. Simulation results verify that the proposed algorithm significantly outperforms other benchmark algorithms.

Index Terms—Spectrum sharing, radar-communication coexistence, joint transceiver design, full-duplex relay.

I. INTRODUCTION

To improve the communication quality-of-service (QoS), wireless systems are traditionally designed to pursue a high data rate and low latency. However, with the rapid development of the artificial intelligence technique, network intelligence has become a new trend of wireless communications [1]. Collecting massive and accurate sensing data is necessary to fulfill the goal of network intelligence [2]. Thus, deploying the radar sensing system within wireless networks has attracted wide public concern. Specifically, the radar system aims to achieve high location accuracy and detection capability [3]. However, these requirements would consume a large amount of bandwidth [31]. Meanwhile, there will be over 30 billion connected devices in use by 2022, which will cause a shortage of bandwidth to serve all communication devices. Thus it is desirable to exploit the bandwidth currently assigned to radar systems. The possibility of spectrum sharing between the communication and radar systems has recently aroused much research interest [5].

However, spectrum sharing will bring new problems, i.e., the mutual interference when the radar and communication systems work simultaneously. To avoid interference and ensure the performance of both systems, the coexistence of separated radar and communication systems has been investigated recently [6]–[12]. In [6], a communication-centric approach was proposed to avoid interference caused by the radar by projecting the radar signal to the null space of the interference channel between the radar and base station (BS). However, it highly affects the performance of the radar system. To guarantee the signal-to-interference-plus-noise ratio (SINR) for the radar system, the authors in [7] designed the transmit covariance matrix of the communication system by minimizing the effective interference power (EIP) at the multiple-input multiple-output (MIMO) radar receiver under the QoS constraint. In [8], the authors developed a complexity-reduction iterative algorithm to increase the SINR at the radar receiver in the radar-communication coexistence system. The work of [9] aimed at maximizing the communication throughput under the SINR constraint at the radar receiver in a multi-carrier coexistence system. The minimization of transmit power and interference from the BS to radar was studied in [10] for the coexistence of radar and multi-user communication systems. In [11], the authors focused on the imperfect channel state information (CSI) and developed a robust MIMO beamforming algorithm to

Y. He, Y. Cai, and G. Yu are with the College of Information Science and Electronic Engineering, Zhejiang University, Hangzhou 310027, China, and also with Zhejiang Provincial Key Laboratory of Information Processing, Communication and Networking (IPCAN), Hangzhou 310027, China (e-mail: {2014hyh, ylcai, yuguanding}@zju.edu.cn).

K. K. Wong is with the Department of Electronic and Electrical Engineering, University College London, London WC1E 6BT, U.K. (e-mail: kai-kit.wong@ucl.ac.uk).

maximize the radar detection probability. Both the max-min and weighted-sum criteria were considered in [12] to solve the problem of timing uncertainty caused by the uncertain target locations.

In addition to the coexistence of the separated radar and communications systems, there is another scheme, namely, the dual-functional radar-communication (DFRC) system [13], where the radar and BS share the same radio frequency (RF) hardware equipment. Compared with separated systems, DFRC systems can save the hardware overhead while making full use of bandwidth. Most recent studies about DFRC systems focus on the design of transceiver and waveform [14]–[18]. In [14], the authors introduced the estimation rate for radar, namely, the minimum number of bits required to encode the Kalman residual. They derived a performance bound for the DFRC system. The authors of [15] studied a multi-user DFRC system and designed a transmit waveform for the radar function while guaranteeing the downlink communication performance. They also verified the performance advantage of the DFRC system over the conventional separated deployment. In [16], the tradeoff between the radar and communication performance under the power constraint was investigated for the multi-user DFRC system. The authors of [17] developed a multi-user interference mitigation algorithm to solve the issue of high peak average power ratio (PAPR) in the DFRC system. Moreover, a novel transceiver architecture for joint target search and channel estimation was proposed in [18] for the DFRC system.

The aforementioned studies only investigate the coexistence between the radar and BS. On the other hand, future communications may suffer from severe pathloss due to the use of high-frequency bands. To overcome this problem, relay station has been widely developed to improve communication performance [19]. Hence, the study of relay assisted communications is of great importance. Traditional relaying schemes, such as amplify-and-forward (AF) [20], [21] and decode-and-forward (DF) [22] protocols, operate in half-duplex (HD) mode, which requires separate time or frequency resources for transmission and reception. By contrast, a full-duplex (FD) relay can potentially double the system capacity by supporting simultaneous transmission and reception [23]–[26]. The work of [23] proposed a low-complexity joint precoding/decoding scheme in a single-stream FD MIMO AF relay system. In [24], source-relay precoding methods for achieving rate maximization were jointly investigated in FD MIMO relaying systems with the assumption of no residual self-interference (SI). Furthermore, the authors in [25] considered the relay processing delay and developed a penalty-based algorithmic framework by joint source transmit beamforming and relay processing. Besides, the millimeter wave (mmWave) FD MIMO relay system was considered in [26], and a robust algorithm was proposed to deal with the CSI error by jointly designing hybrid beamforming matrices. In [27], a joint beamforming, positioning, and power control scheme for a mmWave FD UAV relay was proposed to maximize the achievable rate.

To the best of our knowledge, the integration of radar and relay communication systems has not been well investigated in the literature. The integration of radar and relay can save the hardware overhead while making full use of bandwidth. Meanwhile, the existing solutions for the integration of radar and BS cannot be directly applied since the relay communication system is different from the BS communication system. Furthermore, implementing a dual-functional relay is more practical and easier than implementing a dual-functional BS since the former one does not need to modify the existing communication protocol and architecture while the latter one requires a lot of modifications to the current standards and would bring a high cost. Therefore, in this work, we investigate a novel dual-functional FD relay aided radar-communication system, where the phased-array radar and the AF relay share the same RF hardware and frequency bandwidth for reducing the overhead. Our goal is to maximize the minimum SINR at the radar receiver among all detection directions. The main challenge here is the mutual interference between the radar and relay communications, which may seriously affect the performance. To mitigate it, we jointly design the transceiver of both radar and relay. Further, the SINR at the radar receiver can be improved while satisfying the requirements of communication QoS and total energy.

The main contributions of this paper are summarized as follows.

- The integration of the radar system and relay communication is studied for the first time. Specifically, we propose a dual-functional FD relay aided radar-communication system and formulate a joint transceiver design problem for maximizing the minimum SINR at the radar receiver among all detection directions under the constraints of total energy and communication QoS.
- The formulated problem is very challenging to tackle directly. Based on the special problem structure, we equivalently decompose it into two kinds of subproblems that are more tractable, i.e., the relay-energy and radar-energy minimization problems.
- A joint transceiver design algorithm is proposed based on solving the resultant subproblems. Specifically, we develop a low-complexity algorithm based on the alternating direction method of multipliers (ADMM) for optimizing the transmit power and receiver for radar function to minimize the radar energy and derive a closed-form solution of the AF beamforming matrix to the relay-energy minimization problem.
- We analyze the optimality and computational complexity of the proposed algorithm. Our simulation results demonstrate the performance advantages of the proposed algorithm over other benchmark designs.

The rest of the paper is organized as follows. Section II introduces the system model and mathematically formulates the problem of interest. In Section III, the investigated

(a) System scenario.
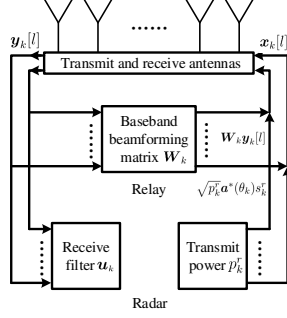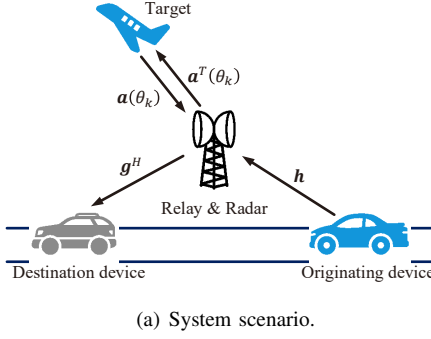

(b) The RF architecture for both radar and relay.

Fig. 1. Dual-functional FD relay aided radar-communication system. Each RF chain can be implemented with a high-precision digital-to-analog converter (or analog-to-digital converter), a digital up converter (or digital down converter), and a power amplifier with a broad linear range [28], [29].

problem is equivalently decomposed into more tractable subproblems. In Section IV, we introduce the proposed joint transceiver design algorithm by solving the resultant subproblems. The simulation results are shown in Section V, and Section VI concludes the paper.

Notations: In this paper, scalars, vectors, and matrices are denoted by lower case, boldface lower case, and boldface upper case letters, respectively. $\boldsymbol{I}$ represents an identity matrix and $\boldsymbol{0}$ denotes an all-zero vector. $(\cdot)^*$, $(\cdot)^T$, and $(\cdot)^H$ denote complex conjugate, transpose, and Hermitian transpose, respectively. For a matrix $\boldsymbol{A}$, $||\boldsymbol{A}||$ denotes its Frobenius norm. For a square matrix $\boldsymbol{A}$, $\mathrm{tr}(\boldsymbol{A})$ denotes its trace. For a vector $\boldsymbol{a}$, $||\boldsymbol{a}||$ represents its Euclidean norm. $\mathbb{C}^{m \times n}$ denotes the space of $m \times n$ complex matrices.

II. SYSTEM MODEL AND PROBLEM FORMULATION

As depicted in Fig. 1, we consider a dual-functional FD relay aided radar-communication system, where an FD AF MIMO relay and a phased-array radar share a common uniform linear array (ULA) with M transmit and M receive antennas, respectively. Both relay and radar transmit on the same frequency band. In the system, the relay forwards the communication signal from the originating device to the destination device. For simplicity, we assume that devices are equipped with a single antenna[1].

Thus, the transmit and received signals at the common ULA are dual-functional. Meanwhile, as shown in Fig. 2,

[1]In order to focus on our study, we consider a typical case of single-antenna devices, whereas the results in this paper can be extended to the general setup of multi-antenna devices, which is left for future work.
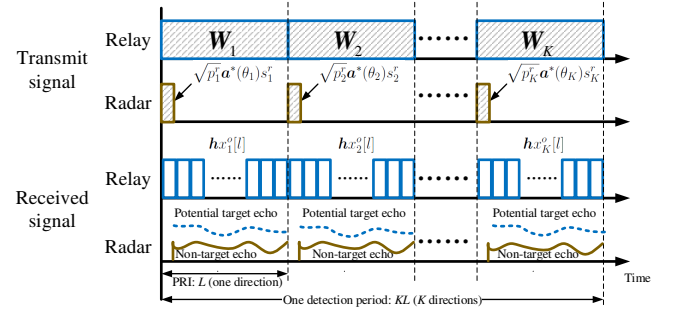

Fig. 2. Dual-functional transmit and received signals at the common ULA.

the phased-array radar detects the targets in K directions successively within a detection period. Denote L as the pulse repetition interval (PRI), which is the transmit-receive cycle for one detection direction.[2] Thus, the duration of a detection period is KL. The baseband beamforming matrix of the relay, denoted by $\boldsymbol{W}_k \in \mathbb{C}^{M \times M}$, the receive filter of the radar, denoted by $\boldsymbol{u}_k \in \mathbb{C}^{M \times 1}$, and the transmit power of the radar, denoted by p_k^r, all vary with the detection direction.

A. Radar and Relay Communication Models

For radar function, let θ_k denote the k-th detection direction, $k \in \mathbb{K} \triangleq \{1, \ldots, K\}$. As shown in Fig. 2, during the detection process for direction θ_k, the time index 0, i.e., $l = 0$, is utilized for transmitting the probing pulse and the remaining time indices, denoted by $\mathbb{L} = \{1, 2, \cdots, L-1\}$, are employed for waiting and detecting the echo [30]. Based on this, we can analyze the following two cases.

1) When time index $l = 0$, there is no echo and the received signal at the common ULA only contains the transmit signal from the originating device[3], denoted by $x_k^o[l]$, which is given by

$$\boldsymbol{y}_k[l] = \boldsymbol{h} x_k^o[l] + \boldsymbol{n}[l], \quad l = 0, \tag{1}$$

where $\boldsymbol{h} \in \mathbb{C}^{M \times 1}$ is the channel vector between the originating device and the relay and $\boldsymbol{n}[l] \sim \mathcal{CN}\left(0, \sigma^2 \boldsymbol{I}\right)$ is the complex circular Gaussian noise vector with zero mean and covariance $\mathbb{E}\left\{\boldsymbol{n}[l] \boldsymbol{n}^H[l]\right\} = \sigma^2 \boldsymbol{I}$, including the residual SI and the additive white Gaussian noise.[4]

As for the transmit signal, the probing pulse of the radar towards the detection direction θ_k is $\sqrt{p_k^r} \boldsymbol{a}^*(\theta_k) s_k^r$, where $\boldsymbol{a}(\theta) = \frac{1}{\sqrt{M}}\left[1, e^{j2\frac{\pi}{\lambda_o}\Delta\sin(\theta)}, \cdots, e^{j2\frac{\pi}{\lambda_o}(M-1)\Delta\sin(\theta)}\right]^T \in \mathbb{C}^{M \times 1}$ with λ_o being the wavelength and Δ being the

[2]To detect all targets of interest, L should be long enough [31]. Suppose there is a target located beyond the maximum distance. In that case, the corresponding echo can be modeled as noise since it is too far and the power of the echo is too low to be neglected.

[3]We consider a wireless cellular system in this paper, where the relay is the control center and all devices in the system are time-synchronized. This can be achieved by GNSS-based time synchronization using standard GPS service [32].

[4]The SI can be canceled with certain interference cancellation techniques [33]–[35]. According to [36], the power of the residual SI at the relay and radar approaches that of the additive white noise and can be modeled as complex circular Gaussian noise [37], [38] since the CSI of the SI link can be obtained, as well as the relay and radar share the same hardware and information. Note that the same assumption has been widely adopted in several other related works, such as [39].

antenna spacing, and s_k^r is the transmit radar symbol with $\mathbb{E}\left\{s_k^r(s_k^r)^H\right\} = 1$. Without loss of generality, we set $\Delta = \lambda_o/2$. Thus, the dual-functional transmit signal at the common ULA can be expressed as

$$\boldsymbol{x}_k[l] = \underbrace{\boldsymbol{W}_k\left(\boldsymbol{h}x_k^o[l] + \boldsymbol{n}[l]\right)}_{\text{communication signal}} + \underbrace{\sqrt{p_k^r}\boldsymbol{a}^*(\theta_k)s_k^r}_{\text{probing pulse}}, \ l = 0. \quad (2)$$

Let $\boldsymbol{g} \in \mathbb{C}^{M \times 1}$ denote the channel vector between the destination device and the relay. Then, the received signal at the destination device is given by

$$y_k^c[l] = \boldsymbol{g}^H\left(\boldsymbol{W}_k\left(\boldsymbol{h}x_k^o[l] + \boldsymbol{n}[l]\right) + \sqrt{p_k^r}\boldsymbol{a}^*(\theta_k)s_k^r\right) + n^c[l], \quad l = 0, \quad (3)$$

where $n^c[l] \sim \mathcal{CN}\left(0, \sigma^2\right)$ is the circular Gaussian noise with zero mean and variance of σ^2.

2) For time index $l \in \mathbb{L}$, the transmit probing pulse is reflected by the potential target back to the radar along with the detection direction θ_k. We assume that there is a potential target echo that arrives at the common ULA at each time index $l \in \mathbb{L}$ since we have no prior knowledge about the target. In addition, it is also reflected by other obstacles in the surrounding environment. Without loss of generality, we assume that the radar has prior knowledge about the surrounding environment, which can be obtained by early detection. The potential echo signal at the receiver at time index l is given by

$$\boldsymbol{y}_k^r[l] = \underbrace{\sqrt{p_k^r}\alpha_k[l]\boldsymbol{a}(\theta_k)\boldsymbol{a}^T(\theta_k)\boldsymbol{a}^*(\theta_k)s_k^r}_{\text{target echo}} + \underbrace{\sqrt{p_k^r}\boldsymbol{A}[l]\boldsymbol{a}^*(\theta_k)s_k^r}_{\text{non-target echo}}$$
$$= \sqrt{p_k^r}\alpha_k[l]\boldsymbol{a}(\theta_k)s_k^r + \sqrt{p_k^r}\boldsymbol{A}[l]\boldsymbol{a}^*(\theta_k)s_k^r, \ l \in \mathbb{L}, \quad (4)$$

where $\alpha_k[l]$ represents the complex path loss including propagation loss and reflection coefficient along with the detection direction θ_k at the time index l and $\boldsymbol{A}[l] = \sum_{i=1}^{I_l} \kappa_i[l]\boldsymbol{a}(\theta_{l,i})\boldsymbol{a}^T(\theta_{l,i}) \in \mathbb{C}^{M \times M}$ denotes the corresponding channel matrix of I_l non-target obstacles with $\kappa_i[l]$ being the path loss and $\theta_{l,i}$ being the angle. Note that $\alpha_k[l]$ is determined by its time index l and can be estimated with an empirical model.

Considering the transmit signal from the originating device, the overall received signal at the common ULA is

$$\boldsymbol{y}_k[l] = \boldsymbol{h}x_k^o[l] + \sqrt{p_k^r}\alpha_k[l]\boldsymbol{a}(\theta_k)s_k^r + \sqrt{p_k^r}\boldsymbol{A}[l]\boldsymbol{a}^*(\theta_k)s_k^r + \boldsymbol{n}[l], \quad l \in \mathbb{L}. \quad (5)$$

The corresponding dual-functional transmit signal at the common ULA is

$$\boldsymbol{x}_k[l] = \boldsymbol{W}_k\boldsymbol{y}_k[l], \quad l \in \mathbb{L}. \quad (6)$$

It contains the potential target echo near the common ULA, which interferes with the communication signal seriously. Hence, to guarantee the communication QoS, we force $\boldsymbol{W}_k$ to lie in the null space of $\boldsymbol{a}(\theta_k)$, i.e., $\boldsymbol{W}_k\boldsymbol{a}(\theta_k) = \boldsymbol{0}, \forall k$. This assumption also helps us gain more insights on the design of relay beamforming. Moreover, constraint

$\boldsymbol{W}_k\boldsymbol{a}(\theta_k) = \boldsymbol{0}, \forall k$ does not need perfect CSI and thus can be achieved easily in practice.

Then, the dual-functional transmit signal can be rewritten as

$$\boldsymbol{x}_k[l] = \boldsymbol{W}_k\left(\boldsymbol{h}x_k^o[l] + \sqrt{p_k^r}\boldsymbol{A}[l]\boldsymbol{a}^*(\theta_k)s_k^r + \boldsymbol{n}[l]\right), l \in \mathbb{L}. \quad (7)$$

Therefore, the received signal at the destination device is

$$y_k^c[l] = \boldsymbol{g}^H\boldsymbol{W}_k\left(\boldsymbol{h}x_k^o[l] + \sqrt{p_k^r}\boldsymbol{A}[l]\boldsymbol{a}^*(\theta_k)s_k^r + \boldsymbol{n}[l]\right) + n^c[l], \quad l \in \mathbb{L}. \quad (8)$$

Combining the above two cases, we can conclude that the total received signal at the common ULA is

$$\boldsymbol{y}_k[l] = \begin{cases} \boldsymbol{h}x_k^o[l] + \boldsymbol{n}[l], & l = 0, \\ \boldsymbol{h}x_k^o[l] + \sqrt{p_k^r}\alpha_k[l]\boldsymbol{a}(\theta_k)s_k^r & \\ \quad + \sqrt{p_k^r}\boldsymbol{A}[l]\boldsymbol{a}^*(\theta_k)s_k^r + \boldsymbol{n}[l], & l \in \mathbb{L}, \end{cases} \quad (9)$$

the corresponding dual-functional transmit signal at the common ULA is

$$\boldsymbol{x}_k[l] = \begin{cases} \boldsymbol{W}_k\left(\boldsymbol{h}x_k^o[l] + \boldsymbol{n}[l]\right) & \\ \quad + \sqrt{p_k^r}\boldsymbol{a}^*(\theta_k)s_k^r, & l = 0, \\ \boldsymbol{W}_k\left(\boldsymbol{h}x_k^o[l] + \boldsymbol{n}[l]\right) & \\ \quad + \boldsymbol{W}_k\sqrt{p_k^r}\boldsymbol{A}[l]\boldsymbol{a}^*(\theta_k)s_k^r, & l \in \mathbb{L}, \end{cases} \quad (10)$$

and the total received signal at the destination device is

$$y_k^c[l] = \begin{cases} \boldsymbol{g}^H\boldsymbol{W}_k\left(\boldsymbol{h}x_k^o[l] + \boldsymbol{n}[l]\right) + n^c[l] & \\ \quad + \sqrt{p_k^r}\boldsymbol{g}^H\boldsymbol{a}^*(\theta_k)s_k^r, & l = 0, \\ \boldsymbol{g}^H\boldsymbol{W}_k\left(\boldsymbol{h}x_k^o[l] + \boldsymbol{n}[l]\right) + n^c[l] & \\ \quad + \boldsymbol{g}^H\boldsymbol{W}_k\sqrt{p_k^r}\boldsymbol{A}[l]\boldsymbol{a}^*(\theta_k)s_k^r, & l \in \mathbb{L}, \end{cases} \quad (11)$$

B. Energy Consumption and SINR

Based on the above analysis, the energy consumption of the radar function and the relay communication function for the direction θ_k can be given by

$$E_k^r = p_k^r, \quad (12)$$
$$E_k^c = Lp^c \left\|\boldsymbol{W}_k\boldsymbol{h}\right\|^2 + L\sigma^2 \left\|\boldsymbol{W}_k\right\|^2$$
$$\quad + p_k^r \sum_{l \in \mathbb{L}} \left\|\boldsymbol{W}_k\boldsymbol{A}[l]\boldsymbol{a}^*(\theta_k)\right\|^2$$
$$= Lp^c \left\|\boldsymbol{W}_k\boldsymbol{h}\right\|^2 + L\sigma^2 \left\|\boldsymbol{W}_k\right\|^2$$
$$\quad + p_k^r \text{tr}\left(\boldsymbol{W}_k\boldsymbol{P}_k\boldsymbol{W}_k^H\right), \quad (13)$$

respectively, where $\boldsymbol{P}_k \triangleq \sum_{l \in \mathbb{L}} \boldsymbol{A}[l]\boldsymbol{a}^*(\theta_k)\boldsymbol{a}^T(\theta_k)\boldsymbol{A}[l]^H$ is a Hermitian matrix, i.e., $\boldsymbol{P}_k^H = \boldsymbol{P}_k$, and $p^c = \mathbb{E}\left\{x_k^o[l]^*x_k^o[l]\right\}$. Equation (12) is given based on the fact that the radar only transmits pulse at time index $l = 0$ for direction θ_k.

For the radar function, the received signal is first operated by the receive filter $\boldsymbol{u}_k$, which can suppress the interference from the communication signal. Then, the processed signal is utilized for target detection. At time index l for direction θ_k, the target detection process can be described as a binary

hypothesis testing problem, which is given by

$$\begin{cases} \mathcal{H}_0: \; \boldsymbol{u}_k \left(\boldsymbol{h} x_k^o[l] + \sqrt{p_k^r} \boldsymbol{A}[l] \boldsymbol{a}^*(\theta_k) s_k^r + \boldsymbol{n}[l] \right), \\ \mathcal{H}_1: \; \boldsymbol{u}_k \left(\sqrt{p_k^r} \alpha_k[l] \boldsymbol{a}(\theta_k) s_k^r + \boldsymbol{h} x_k^o[l] \right. \\ \qquad \left. + \sqrt{p_k^r} \boldsymbol{A}[l] \boldsymbol{a}^*(\theta_k) s_k^r + \boldsymbol{n}[l] \right). \end{cases} \quad (14)$$

According to [8], we can adopt the minimum SINR at the radar receiver among all time indices $l \in \mathbb{L}$ to represent the radar detection performance for the direction θ_k, which is given by

$$\mathrm{SINR}_k^r =$$
$$\min_{l \in \mathbb{L}} \left\{ \frac{p_k^r \left| \boldsymbol{u}_k^H \alpha_k[l] \boldsymbol{a}(\theta_k) \right|^2}{p_k^r \left| \boldsymbol{u}_k^H \boldsymbol{A}[l] \boldsymbol{a}^*(\theta_k) \right|^2 + p^c \left| \boldsymbol{u}_k^H \boldsymbol{h} \right|^2 + \sigma^2 \left\| \boldsymbol{u}_k \right\|^2} \right\}. \quad (15)$$

As for the relay communication function, the average SINR of the received signal $y_k^c[l]$ for the direction θ_k is given by

$$\mathrm{SINR}_k^c =$$
$$\frac{L p^c \left| \boldsymbol{g}^H \boldsymbol{W}_k \boldsymbol{h} \right|^2}{p_k^r \left(\left| \boldsymbol{g}^H \boldsymbol{a}^*(\theta_k) \right|^2 + \boldsymbol{g}^H \boldsymbol{W}_k \boldsymbol{P}_k \boldsymbol{W}_k^H \boldsymbol{g} \right) + L\sigma^2 \left\| \boldsymbol{g}^H \boldsymbol{W}_k \right\|^2 + L\sigma^2}. \quad (16)$$

C. Problem Formulation

In this work, we aim to maximize the minimum SINR at the radar receiver among all directions under the constraints of relay communication QoS and total energy within a detection period to improve the overall detection performance of the radar function. Therefore, the problem can be mathematically formulated as

$$\max_{\{\boldsymbol{W}_k, \boldsymbol{u}_k, p_k^r\}} \quad \min_k \left\{ \mathrm{SINR}_k^r \right\}, \quad (17a)$$
$$\text{s.t.} \quad \mathrm{SINR}_k^c \geq \gamma^c, \forall k, \quad (17b)$$
$$\boldsymbol{W}_k \boldsymbol{a}(\theta_k) = \boldsymbol{0}, \forall k, \quad (17c)$$
$$\sum_{k=1}^K \left(E_k^c + E_k^r \right) \leq E^u, \quad (17d)$$

where the constraint (17b) ensures the communication performance, constraint (17c) avoids the potential interference caused by the target echo signal from the radar, and constraint (17d) limits the total transmit energy consumption. In the above, $\gamma^c > 0$ denotes the communication SINR requirement and E^u is the total transmit energy budget. Note that the interference from the destination device and non-target echo would have different effects on the radar performance with different detection directions. Thus, to improve the overall radar detection performance, we need to couple all K directions together by giving a total energy limitation instead of independent power constraints. For practical consideration, we normalize the optimal receiver vector after solving problem (17), and thus there is no power constraint for $\boldsymbol{u}_k$.

It can be observed that problem (17) is very challenging. In the following section, we will equivalently decompose it

into two more tractable subproblems and develop effective algorithms to solve them, respectively.

III. PROBLEM DECOMPOSITION

To tackle the highly nonlinear objective function of problem (17), we first analyze the relationship between the total energy budget E^u and the optimal objective value, denoted by $\gamma^{r,\star}$, as shown in the following lemma.

Lemma 1: $\gamma^{r,\star}$ is monotonically non-decreasing with E^u ($E^u > 0$).

Proof: As E^u increases, the feasible set becomes larger. Thus, the optimal objective value would not decrease with E^u, which ends the proof. ∎

Based on Lemma 1, we can consider a dual problem that minimizes the total transmit energy with a given SINR requirement at the radar receiver, denoted by γ^r, as

$$\min_{\{\boldsymbol{W}_k, \boldsymbol{u}_k, p_k^r\}} \quad \sum_{k=1}^K \left(E_k^c + E_k^r \right), \quad (18a)$$
$$\text{s.t.} \quad \mathrm{SINR}_k^r \geq \gamma^r, \forall k, \quad (18b)$$
$$(17b) \text{ and } (17c). \quad$$

Let $E^\star(\gamma^r)$ denote the optimal objective value of problem (18) when the SINR requirement at the radar receiver is γ^r. Then, by exhaustively searching on γ^r, we can find $\gamma^{r,\star}$ that satisfies $E^\star(\gamma^{r,\star}) = E^u$, which is the optimal objective value of problem (17) based on Lemma 1. Also, the corresponding solution to the problem (18) is the optimal solution to problem (17).

To proceed, we focus on problem (18) and decouple it into K independent problems for K directions, which can be solved in parallel. Each problem is given by

$$\min_{\substack{\boldsymbol{W}_k, \\ \boldsymbol{u}_k, p_k^r}} \quad p_k^r + L p^c \left\| \boldsymbol{W}_k \boldsymbol{h} \right\|^2 + L\sigma^2 \left\| \boldsymbol{W}_k \right\|^2$$
$$+ p_k^r \mathrm{tr} \left(\boldsymbol{W}_k \boldsymbol{P}_k \boldsymbol{W}_k^H \right), \quad (19a)$$
$$\text{s.t.} \quad p_k^r \left| \boldsymbol{u}_k^H \alpha_k[l] \boldsymbol{a}(\theta_k) \right|^2 / \left(p_k^r \left| \boldsymbol{u}_k^H \boldsymbol{A}[l] \boldsymbol{a}^*(\theta_k) \right|^2 \right.$$
$$\left. + p^c \left| \boldsymbol{u}_k^H \boldsymbol{h} \right|^2 + \sigma^2 \left\| \boldsymbol{u}_k \right\|^2 \right) \geq \gamma^r, \forall l \in \mathbb{L}, \quad (19b)$$
$$L p^c \left| \boldsymbol{g}^H \boldsymbol{W}_k \boldsymbol{h} \right|^2 / \left(p_k^r \left| \boldsymbol{g}^H \boldsymbol{a}^*(\theta_k) \right|^2 \right.$$
$$+ p_k^r \boldsymbol{g}^H \boldsymbol{W}_k \boldsymbol{P}_k \boldsymbol{W}_k^H \boldsymbol{g} + L\sigma^2 \left\| \boldsymbol{g}^H \boldsymbol{W}_k \right\|^2$$
$$\left. + L\sigma^2 \right) \geq \gamma^c, \quad (19c)$$
$$\boldsymbol{W}_k \boldsymbol{a}(\theta_k) = \boldsymbol{0}. \quad (19d)$$

The objective function of the problem (19) contains the energy of both the radar function and relay communication function. The optimization variables can also be divided into two parts, i.e., $\boldsymbol{u}_k$ and p_k^r for the radar function and $\boldsymbol{W}_k$ for the relay communication function. Therefore, we can further equivalently decompose this problem into two subproblems. First, we solve the radar-energy minimization problem by optimizing $\boldsymbol{u}_k$ and p_k^r, as

$$\min_{\{\boldsymbol{u}_k, p_k^r\}} \quad p_k^r, \quad (20)$$

s.t.   (19b).

After obtaining the optimal solution to problem (20), denoted by $\boldsymbol{u}_k^\star$ and $p_k^{r,\star}$, we then solve the relay-energy minimization problem with $p_k^r = p_k^{r,\star}$, as

$$\min_{\{\boldsymbol{W}_k\}} \quad Lp^c \left\|\boldsymbol{W}_k\boldsymbol{h}\right\|^2 + L\sigma^2 \left\|\boldsymbol{W}_k\right\|^2$$
$$+ p_k^r \mathrm{tr}\left(\boldsymbol{W}_k\boldsymbol{P}_k\boldsymbol{W}_k^H\right), \qquad (21)$$
$$\text{s.t.} \quad \text{(19c) and (19d).}$$

We denote the optimal solution to (21) by $\boldsymbol{W}_k^\star$. By analyzing the intrinsic relations between the problem (19) and these two subproblems, we have the following theorem.

Theorem 1: The solution $\left\{\boldsymbol{u}_k^\star, p_k^{r,\star}, \boldsymbol{W}_k^\star\right\}$ obtained from problems (20) and (21) is the optimal solution to problem (19).

Proof: Please refer to Appendix A. ∎

Remark 1: In constraint (19b), the interference to the radar caused by the relay communication is $p^c \left|\boldsymbol{u}_k^H\boldsymbol{h}\right|^2$, which is a constant. Therefore, we can first consider the radar-energy minimization problem and find the optimal solution $\left\{\boldsymbol{u}_k^\star, p_k^{r,\star}\right\}$. Moreover, the interference to the relay communication caused by the radar includes $p_k^r \left|\boldsymbol{g}^H\boldsymbol{a}^*(\theta_k)\right|^2$ and $p_k^r \boldsymbol{g}^H\boldsymbol{W}_k\boldsymbol{P}_k\boldsymbol{W}_k^H\boldsymbol{g}$ in constraint (19c). To reduce the interference, p_k^r should be minimized, which is also the objective function of the radar-energy minimization problem. Hence, p_k^r should be equivalent to $p_k^{r,\star}$ in the relay-energy minimization problem. After solving two problems successively, the optimal solution to problem (19) can be obtained as shown in Theorem 1. In a nutshell, we can obtain the optimal solution to problem (18) by respectively solving the radar-energy and relay-energy minimization problems for each detection direction.

IV. JOINT TRANSCEIVER DESIGN

In this section, we propose the joint transceiver design algorithm by solving the resultant radar-energy and relay-energy minimization problems. Then, we analyze the optimality and computational complexity of the proposed algorithm.

A. Radar-Energy Minimization

To solve the radar-energy minimization problem shown in (20), we first equivalently transform it into an easier handling form. Let us introduce the following lemma.

Lemma 2: By introducing $\chi_k \triangleq \dfrac{p^c \left|\boldsymbol{u}_k^H\boldsymbol{h}\right|^2 + \sigma^2 \left\|\boldsymbol{u}_k\right\|^2}{p_k^r}$, problem (20) is equivalent to the following convex problem in the sense that the optimal solutions of $\boldsymbol{u}_k$ and p_k^r for the two problems are identical

$$\min_{\{\boldsymbol{u}_k, \chi_k\}} \quad p_k^r = \frac{p^c \left|\boldsymbol{u}_k^H\boldsymbol{h}\right|^2 + \sigma^2 \left\|\boldsymbol{u}_k\right\|^2}{\chi_k}, \qquad (22a)$$
$$\text{s.t.} \quad \boldsymbol{u}_k^H\boldsymbol{a}(\theta_k) = 1, \qquad (22b)$$

$$\left|\boldsymbol{u}_k^H\boldsymbol{A}_k[l]\boldsymbol{a}^*(\theta_k)\right|^2 + \chi_k \leq \frac{\left|\alpha_k[l]\right|^2}{\gamma^r}, \forall l \in \mathbb{L}. (22c)$$

Proof: Please refer to Appendix B. ∎

Based on Lemma 2, although the interior point method, e.g., CVX [40], can be utilized to solve problem (22), it requires high computational complexity due to the multiple large-dimensional constraints in (22c). To this end, in this section, we develop a low-complexity algorithm based on the ADMM optimization framework.

We note that the variables $\boldsymbol{u}_k$ and χ_k appear in a number of different constraints in (22c). Therefore, in order to perform the ADMM method [41]–[43], we introduce the auxiliary variables $\widehat{\boldsymbol{u}}_{k,l}$ and $\widehat{\chi}_{k,l}, \forall l \in \mathbb{L}$, which meet the following linearly coupled equality (LCE) constraints

$$\widehat{\boldsymbol{u}}_{k,l} = \boldsymbol{u}_k, \quad \widehat{\chi}_{k,l} = \chi_k, \quad \forall l \in \mathbb{L}. \qquad (23)$$

Then, constraint (22c) can be expressed as

$$\left|\widehat{\boldsymbol{u}}_{k,l}^H\boldsymbol{A}_k[l]\boldsymbol{a}^*(\theta_k)\right|^2 + \widehat{\chi}_{k,l} \leq \frac{\left|\alpha_k[l]\right|^2}{\gamma^r}, \forall l \in \mathbb{L}. \qquad (24)$$

Therefore, problem (22) can be equivalently converted into

$$\min_{\{\boldsymbol{u}_k, \chi_k, \widehat{\boldsymbol{u}}_{k,l}, \widehat{\chi}_{k,l}\}} \quad \frac{p^c \left|\boldsymbol{u}_k^H\boldsymbol{h}\right|^2 + \sigma^2 \left\|\boldsymbol{u}_k\right\|^2}{\chi_k}, \qquad (25)$$
$$\text{s.t.} \quad \text{(22b), (23), and (24).}$$

By dualizing and penalizing the LCE constraints into the objective function with Lagrange multipliers: $\boldsymbol{\lambda}_{k,l}$ and $\nu_{k,l}$, we can obtain the following augmented Lagrangian (AL) problem

$$\min_{\{\boldsymbol{u}_k, \chi_k, \widehat{\boldsymbol{u}}_{k,l}, \widehat{\chi}_{k,l}\}} \quad \mathcal{L}_\rho\left(\mathbb{Z}_1, \mathbb{Z}_2; \boldsymbol{\lambda}_{k,l}, \nu_{k,l}\right)$$
$$= \frac{p^c \left|\boldsymbol{u}_k^H\boldsymbol{h}\right|^2 + \sigma^2 \left\|\boldsymbol{u}_k\right\|^2}{\chi_k}$$
$$+ \frac{\rho}{2}\sum_{l \in \mathbb{L}} \left\|\boldsymbol{u}_k - \widehat{\boldsymbol{u}}_{k,l} + \frac{1}{\rho}\boldsymbol{\lambda}_{k,l}\right\|^2$$
$$+ \frac{\rho}{2}\sum_{l \in \mathbb{L}} \left\|\chi_k - \widehat{\chi}_{k,l} + \frac{1}{\rho}\nu_{k,l}\right\|^2, (26)$$
$$\text{s.t.} \quad \text{(22b) and (24),}$$

where ρ is the penalty parameter. Then, the variables can be divided into two blocks: $\mathbb{Z}_1 = \{\boldsymbol{u}_k, \chi_k\}$ and $\mathbb{Z}_2 = \{\widehat{\boldsymbol{u}}_{k,l}, \widehat{\chi}_{k,l}\}$. With fixing $\mathbb{Z}_2$, the problem in the first block is given by

$$\min_{\{\mathbb{Z}_1\}} \quad \mathcal{L}_\rho\left(\mathbb{Z}_1, \mathbb{Z}_2; \boldsymbol{\lambda}_{k,l}, \nu_{k,l}\right), \qquad (27)$$
$$\text{s.t.} \quad \text{(22b).}$$

Similarly, with fixing $\mathbb{Z}_1$, the problem in the second block is given by

$$\min_{\{\mathbb{Z}_2\}} \quad \mathcal{L}_\rho\left(\mathbb{Z}_1, \mathbb{Z}_2; \boldsymbol{\lambda}_{k,l}, \nu_{k,l}\right), \qquad (28)$$
$$\text{s.t.} \quad \text{(24).}$$

Algorithm 1: Low-Complexity ADMM-Based Algorithm.

1 Initialize all the primal variables $\mathbb{Z}_1$ and $\mathbb{Z}_2$, the AL multipliers $\boldsymbol{\lambda}_{k,l}, \nu_{k,l}$. Set the tolerance of accuracy $\epsilon > 0$, the penalty parameter $\rho > 0$, the current iteration number $i = 0$, and the maximum iteration number $I_{\max}$;

2 repeat

3   Update the variables $\mathbb{Z}_1$ by solving problem (27);

4   Update the variables $\mathbb{Z}_2$ by solving problem (28);

5   Update the multipliers $\boldsymbol{\lambda}_{k,l}$ and $\nu_{k,l}$ according to (29) and (30);

6 $i = i + 1$

7 until The stop criterion is met or $i > I_{\max}$.

The details of the proposed ADMM-based algorithm are presented in Algorithm 1. In each iteration, we first need to solve the above two problems via the Lagrange multiplier method, whose detailed derivation is provided in Appendix C. After that, we need to update the dual variables as

$$\boldsymbol{\lambda}_{k,l}^{i+1} = \boldsymbol{\lambda}_{k,l}^{i} + \rho\left(\boldsymbol{u}_k - \widehat{\boldsymbol{u}}_{k,l}\right), \forall l \in \mathbb{L}, \tag{29}$$

$$\nu_{k,l}^{i+1} = \nu_{k,l}^{i} + \rho\left(\chi_k - \widehat{\chi}_{k,l}\right), \forall l \in \mathbb{L}. \tag{30}$$

According to [41], the ADMM-based algorithm converges to the optimal solution to the radar-energy minimization problem. Besides, it requires a low computational complexity since the problem of the second block can be decomposed into several subproblems, which can be solved in parallel. Regarding problem (27), we need to obtain the closed-form solution with multiplications $\mathcal{O}(M)$ times and the bisection search can be utilized. The number of iterations is $\log_2 \frac{I_0}{\epsilon}$, where I_0 is the initialized interval length and ϵ is the tolerance of accuracy. Thus, the computational complexity of solving problem (27) is $\mathcal{O}\left(M + \log_2 \frac{I_0}{\epsilon}\right)$. Similarly, the computational complexity of solving problem (28) is $\mathcal{O}\left(LM\left(M + \log_2 \frac{I_0}{\epsilon}\right)\right)$. Therefore, the overall computational complexity of Algorithm 1 is $\mathcal{O}\left(I_{\max}LM\left(M + \log_2 \frac{I_0}{\epsilon}\right)\right)$, where $I_{\max}$ is the maximum iteration number of Algorithm 1.

Different from the ADMM-based algorithm, the computational complexity of using the interior point method is dominated by the second-order cone (SOC) constraints. In problem (22), there are $(L-1)$ SOC constraints with dimension M. Therefore, according to [44], the computational complexity is $\mathcal{O}\left(I_{\text{inter}}\left(n_{\text{inter}}\sqrt{2L}\left(M^2L + n_{\text{inter}}^2\right)\right)\right)$, where $n_{\text{inter}} = \mathcal{O}(LM)$ and I_{inter} denotes the number of iterations. By comparing the computational complexity between two algorithms, we can find that the proposed ADMM-based algorithm exhibits a much lower computational complexity.

B. Relay-Energy Minimization

The relay-energy minimization problem is difficult to solve directly. By analyzing the structure of this problem, we find that there are three key vectors, i.e., $\boldsymbol{h}$, $\boldsymbol{a}(\theta_k)$, and $\boldsymbol{g}$. The first two vectors are related to the received signal. Therefore, with the Gram-Schmidt orthogonalization [45], we can utilize $\boldsymbol{h}$ and $\boldsymbol{a}(\theta_k)$ to construct a unitary matrix $\boldsymbol{Q}_k = \left[\boldsymbol{q}_{k,1}, \boldsymbol{q}_{k,2}, \cdots, \boldsymbol{q}_{k,M}\right]$, which satisfies

$$\boldsymbol{q}_{k,1} = \frac{\boldsymbol{h}}{||\boldsymbol{h}||}, \quad \boldsymbol{q}_{k,2} = \frac{\boldsymbol{a}(\theta_k) - (\boldsymbol{q}_{k,1}^H \boldsymbol{a}(\theta_k))\boldsymbol{q}_{k,1}}{\left|\left|\boldsymbol{a}(\theta_k) - (\boldsymbol{q}_{k,1}^H \boldsymbol{a}(\theta_k))\boldsymbol{q}_{k,1}\right|\right|},$$

$$\boldsymbol{q}_{k,m}^H \boldsymbol{q}_{k,j} = \begin{cases} 1, & m = j, \\ 0, & m \neq j. \end{cases} \tag{31}$$

Then, we can define an auxiliary variable, $\mathbf{Z}_k \triangleq \mathbf{Q}_k^H \mathbf{W}_k \mathbf{Q}_k = [\mathbf{z}_{k,1}, \mathbf{z}_{k,2}, \cdots, \mathbf{z}_{k,M}]$, which is the beamforming matrix under the orthogonal basis $\boldsymbol{Q}_k$. Here $\boldsymbol{z}_{k,m} \in \mathbb{C}^{M \times 1}$ denotes the m-th column vector in matrix $\boldsymbol{Z}_k$ for $m \in \{1, \ldots, M\}$. Thus, we have $\mathbf{W}_k = \boldsymbol{Q}_k \mathbf{Z}_k \boldsymbol{Q}_k^H$ and the relay-energy minimization problem (21) can be rewritten as

$$\min_{\{\boldsymbol{z}_{k,m}\}} Lp^c ||\boldsymbol{h}||^2 ||\boldsymbol{z}_{k,1}||^2 + L\sigma^2 \sum_{m=1}^{M} ||\boldsymbol{z}_{k,m}||^2$$

$$+ p_k^r \sum_{i=1}^{M}\sum_{j=1}^{M} \boldsymbol{q}_{k,i}^H \boldsymbol{P}_k \boldsymbol{q}_{k,j} \boldsymbol{z}_{k,j}^H \boldsymbol{z}_{k,i}, \tag{32a}$$

$$\text{s.t.} \quad \gamma^c \left(p_k^r \left|\boldsymbol{g}^H \boldsymbol{a}^*(\theta_k)\right|^2 + L\sigma^2 \sum_{m=1}^{M} \left|\boldsymbol{g}^H \boldsymbol{Q}_k \boldsymbol{z}_{k,m}\right|^2 \right.$$

$$\left. + p_k^r \sum_{i=1}^{M}\sum_{j=1}^{M} \boldsymbol{q}_{k,i}^H \boldsymbol{P}_k \boldsymbol{q}_{k,j} \boldsymbol{z}_{k,j}^H \boldsymbol{Q}_k^H \boldsymbol{g}\boldsymbol{g}^H \boldsymbol{Q}_k \boldsymbol{z}_{k,i} \right.$$

$$\left. + L\sigma^2 \right) \leq Lp^c ||\boldsymbol{h}||^2 \left|\boldsymbol{g}^H \boldsymbol{Q}_k \boldsymbol{z}_{k,1}\right|^2, \tag{32b}$$

$$\boldsymbol{q}_{k,2}^H \boldsymbol{a}(\theta_k)\boldsymbol{z}_{k,2} + \boldsymbol{q}_{k,1}^H \boldsymbol{a}(\theta_k)\boldsymbol{z}_{k,1} = \boldsymbol{0}, \tag{32c}$$

where constraint (32c) is transformed from (17c). Then, by analyzing problem (32), we have the following theorem.

Theorem 2: The optimal solution to problem (32) satisfies

$$\boldsymbol{z}_{k,m} = \beta_{k,m}\boldsymbol{Q}_k^H \boldsymbol{g}, \quad \forall m. \tag{33}$$

Moreover, the corresponding $\boldsymbol{W}_k$ is given by

$$\boldsymbol{W}_k = \boldsymbol{g}[\beta_{k,1} \; \beta_{k,2} \; \cdots \; \beta_{k,M}]\boldsymbol{Q}_k^H. \tag{34}$$

Proof: Please refer to Appendix D. ∎

Remark 2: To obtain the optimal solution, we first construct a unitary matrix $\boldsymbol{Q}_k$, which is mainly obtained based on two vectors, $\boldsymbol{h}$ and $\boldsymbol{a}(\theta_k)$. Note that the former is the
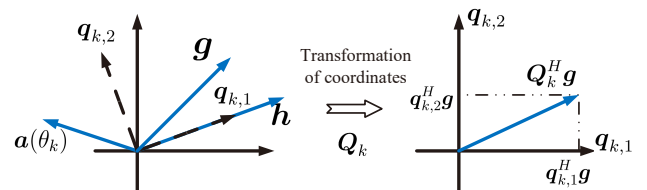

Fig. 3. Transformation of coordinates.

channel vector between the originating device and the relay while the latter is the detection direction vector. Hence, $\boldsymbol{Q}_k$ is jointly determined by both radar and relay. Then, via the transformation of coordinates with the orthogonal basis $\boldsymbol{Q}_k$, we can see that each column of the beamforming matrix should be parallel to $\boldsymbol{Q}_k^H \boldsymbol{g}$ under the orthogonal basis $\boldsymbol{Q}_k$ as shown in Fig. 3. As a result, the beamforming matrix is jointly determined by the communication channel vectors, $\boldsymbol{h}$ and $\boldsymbol{g}$, and the detection direction θ_k.

With Theorem 2, the relay-energy minimization problem can be simplified as

$$\min_{\{\beta_{k,m}\}} \; \left\| \boldsymbol{Q}_k^H \boldsymbol{g} \right\|^2 \left(L p^c \left\| \boldsymbol{h} \right\|^2 \left| \beta_{k,1} \right|^2 + L\sigma^2 \sum_{m=1}^{M} \left| \beta_{k,m} \right|^2 \right.$$
$$\left. + p_k^r \sum_{i=1}^{M} \sum_{j=1}^{M} \boldsymbol{q}_{k,i}^H \boldsymbol{P}_k \boldsymbol{q}_{k,j} \beta_{k,j}^* \beta_{k,i} \right), \quad (35a)$$

$$\text{s.t.} \quad L p^c \left\| \boldsymbol{h} \right\|^2 \left| \beta_{k,1} \right|^2 / \left(\frac{p_k^r \left| \boldsymbol{g}^H \boldsymbol{a}^*(\theta_k) \right|^2 + L\sigma^2}{\left\| \boldsymbol{Q}_k^H \boldsymbol{g} \right\|^4} \right.$$
$$+ p_k^r \sum_{i=1}^{M} \sum_{j=1}^{M} \boldsymbol{q}_{k,i}^H \boldsymbol{P}_k \boldsymbol{q}_{k,j} \beta_{k,j}^* \beta_{k,i}$$
$$\left. + L\sigma^2 \sum_{m=1}^{M} \left| \beta_{k,m} \right|^2 \right) \geq \gamma^c, \quad (35b)$$
$$\boldsymbol{q}_{k,2}^H \boldsymbol{a}(\theta_k) \beta_{k,2} + \boldsymbol{q}_{k,1}^H \boldsymbol{a}(\theta_k) \beta_{k,1} = 0. \quad (35c)$$

By defining $\eta_{k,m} \triangleq \dfrac{\beta_{k,m}}{\beta_{k,1}}, \forall m$, we can further simplify the problem as shown in the following lemma.

Lemma 3: The relay-energy minimization problem is equal to

$$\min_{\{\eta_{k,m}\}} L\sigma^2 \sum_{m=1}^{M} \left| \eta_{k,m} \right|^2 + p_k^r \sum_{i=1}^{M} \sum_{j=1}^{M} \boldsymbol{q}_{k,i}^H \boldsymbol{P}_k \boldsymbol{q}_{k,j} \eta_{k,j}^* \eta_{k,i}, \quad (36)$$

where $\eta_{k,1} = 1$ and $\eta_{k,2} = -\dfrac{\boldsymbol{q}_{k,1}^H \boldsymbol{a}(\theta_k)}{\boldsymbol{q}_{k,2}^H \boldsymbol{a}(\theta_k)}$.

Proof: Please refer to Appendix E. ∎

The above problem is a typical quadratic programming (QP) problem [46] and can be solved by the Lagrange method. Then, the optimal solution is shown in the following theorem.

Theorem 3: Let $\eta_{k,m}^\star$ denote the optimal solution to problem (36) and then it is given as

$$\left[\eta_{k,3}^\star, \cdots, \eta_{k,M}^\star \right] = - \left[\eta_{k,1}, \eta_{k,2} \right] \left[p_k^r \boldsymbol{Q}_k^H \boldsymbol{P}_k \boldsymbol{Q}_k \right]_{1:2,3:M}$$
$$\times \left(L\sigma^2 \boldsymbol{I} + \left[p_k^r \boldsymbol{Q}_k^H \boldsymbol{P}_k \boldsymbol{Q}_k \right]_{3:M,3:M} \right)^{-1}, \quad (37)$$

where the operator $[\cdot]_{m_1:m_2,m_3:m_4}$ represents that extracting the m_1-th to m_2-th rows and the m_3-th to m_4-th columns of the matrix to form a new matrix.

Proof: Please refer to Appendix F. ∎

Remark 3: Based on Theorem 3, we can find that $\eta_{k,m}$ is

---

Algorithm 2: Joint Transceiver Design Algorithm for Solving Problem (17).

---

1 Initialize the maximal error tolerance $\epsilon > 0$ and the range for the SINR at the radar receiver $\gamma_\ell^r = 0, \gamma_u^r = \gamma_{\max}^r$;
2 repeat
3 $\quad$ Let $\gamma^r = (\gamma_\ell^r + \gamma_u^r)/2$;
4 $\quad$ Obtain E_k^r, $\boldsymbol{u}_k$, and p_k^r by utilizing Algorithm 1, $\forall k \in \mathbb{K}$;
5 $\quad$ Obtain E_k^c and $\boldsymbol{W}_k$ according to Theorems 2 and 3, $\forall k \in \mathbb{K}$;
6 $\quad$ **if** $\sum_{k=1}^{K} E_k^r + E_k^c > E^u$ **then**
7 $\quad\quad$ $\gamma_u^r = \gamma^r$;
8 $\quad$ **else**
9 $\quad\quad$ $\gamma_\ell^r = \gamma^r$;
10 $\quad$ **end**
11 until $\left| \sum_{k=1}^{K} E_k^r + E_k^c - E^u \right| < \epsilon$.

---

mainly determined by the radar echo signals. Specifically, $\eta_{k,2}$ is designed in relation to the detection direction θ_k to avoid the interference caused by the target echo signal. $\eta_{k,m}$, $m \in \{3, \cdots, M\}$ is designed to suppress the interference caused by the non-target echo signal.

Based on Theorem 3, we can obtain the minimum relay energy according to (56) and the corresponding beamforming matrix according to Theorem 2.

C. Overall Transceiver Design Algorithm

After solving problem (18), we can employ a bisection search method to obtain the optimal solution to the original problem (17) as we have mentioned before. To perform the bisection search method, we provide the range of the SINR at the radar receiver in the following lemma.

Lemma 4: The upper bound of the SINR at the radar receiver is given by

$$\gamma^r \leq \gamma_{\max}^r = E^u \left(\sum_{k=1}^{K} \left| \alpha_k \right|^{-2} \right) / \sigma^2, \quad (38)$$

where $\left| \alpha_k \right| = \min_{l \in \mathbb{L}} \left| \alpha_k[l] \right|$.

Proof: Please refer to Appendix G. ∎

Then, the overall joint transceiver design algorithm to obtain the optimal SINR $\gamma^{r,\star}$ is shown in Algorithm 2. In this algorithm, the number of iterations for the bisection search is $\log_2 \dfrac{\gamma_{\max}^r}{\epsilon}$. In each iteration, we need to solve the relay-energy and the radar-energy minimization problems for K detection directions, which can be performed in parallel. The computational complexity for solving the relay-energy minimization problem is $\mathcal{O} \left(I_{\max} L M \left(M + \log_2 \dfrac{I_0}{\epsilon} \right) \right)$ as mentioned before. The computational complexity for solving the relay-energy minimization problem is $\mathcal{O} \left(M^3 \right)$ due to the matrix inversion operation for obtaining the optimal $\eta_{k,m}^\star$ in

Theorem 3. Therefore, the overall computational complexity of Algorithm 2 is

$$\mathcal{O}\left(\left(\log_2 \frac{\gamma_{\max}^r}{\epsilon}\right) K \left(I_{\max} LM \left(M + \log_2 \frac{I_0}{\epsilon}\right) + M^3\right)\right).$$

Then, we have the following theorem to ensure the optimality of the proposed algorithm.

Theorem 4: The proposed Algorithm 2 is guaranteed to converge to the optimal solution to problem (17).

Proof: Based on Lemma 1, we can see that the optimal solution to problem (17) can be obtained by utilizing the search method with solving problem (18). Moreover, problem (18) can be decoupled into K independent subproblems for K directions and the optimal solution to each subproblem can be obtained by solving the radar-energy and relay-energy minimization problems as shown in Theorem 1. Therefore, we can conclude that the proposed Algorithm 2 can converge to the optimal solution to the problem (17). The proof is thus completed. ∎

V. SIMULATION RESULTS

In this section, we show the performance of the proposed joint transceiver design algorithm for the dual-functional FD relay aided radar-communication system.

A. Simulation Setup

The simulation settings are summarized as follows unless otherwise specified. The dual-functional relay is equipped with 12 transmit antennas and 12 receive antennas. The center frequency considered in the simulation is 2.4 GHz, the bandwidth is set as 1 MHz, and the noise power is set as -100 dBm. For the radar function, we detect 12 directions within one period, i.e., $0, \frac{1\pi}{36}, \cdots, \frac{11\pi}{36}$, and the PRI is 12. The directions of arrival path of the reflecting echo caused by the non-target objects are randomly generated in $[0, 2\pi)$. As for the path-loss, we model it as: $28.0 + 22.0 \log_{10} d + 20 \log_{10}(f_c)$, where d is the distance in meter and f_c is the center frequency in GHz. The radar-cross-section is set as 1. For the relay communication function, according to [47], the small-scale fading is modeled as $\boldsymbol{h} = \sum_{l_p=1}^{L_p} \alpha_{l_p} \boldsymbol{a}(\theta_{l_p})$, where $L_p = 4$ is the number of distinguishable paths, α_{l_p} is the complex gain of the l_p-th path, and $\theta_{l_p} \in \left[-\frac{\pi}{2}, -\frac{\pi}{6}\right]$ is the azimuth angle of arrival (AoA). The ratio $\frac{||\boldsymbol{h}||^2}{\sigma^2}$ is set as 30 dB. The transmit power of the originating device is set as 20 dBm and the relay SINR requirement is set as 15 dB. The total energy for the radar and relay communication is set as $p^u KL$, where $p^u = 3$ W denotes the average power over a detection period. All algorithms are implemented on a desktop Intel (i7-8700) CPU running at 3.2GHz with 16GB RAM. Note that our proposed algorithm can also show high performance under other simulation parameters.

B. Algorithm Investigation

We first pay attention to the proposed ADMM-based algorithm (Algorithm 1) for the radar-energy minimization
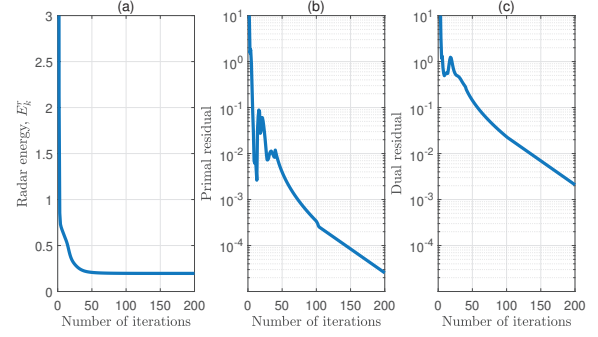

Fig. 4. Convergence behavior of the proposed ADMM-based algorithm.
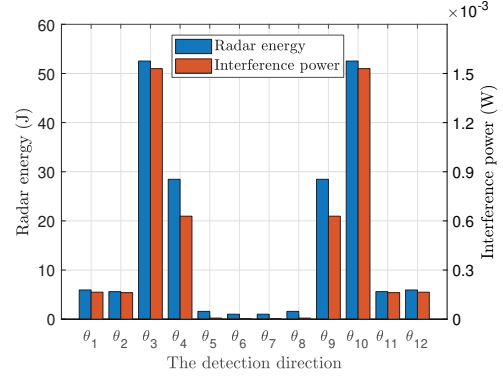

Fig. 5. The energy allocation and the interference caused by the relay communication for each detection direction.

problem. Fig. 4 shows the convergence behavior of the proposed ADMM-based algorithm when the SINR requirement at the radar receiver is 1 dB. It is observed that the proposed algorithm can converge to the optimal solution monotonically within 50 iterations. Besides, both values of the primal residual and dual residual [41] almost decrease with the number of iterations, which further verifies the convergence. Moreover, we also compare the CPU running time and the minimum radar energy of the proposed ADMM-based algorithm with those of the interior point method, i.e., the CVX solver, under different time slot lengths. The results are shown in Table I and Table II, respectively. We can observe that the running time of the proposed ADMM-based algorithm only costs around a tenth of that of the CVX solver while the minimum radar energy of these two methods is almost identical. The results show that the proposed Algorithm 1 achieves almost the same performance as the CVX solver with much reduced computational complexity.

We also investigate the relation between the energy allocation for each detection direction and the interference caused by the relay communication. The results are shown in Fig. 5. We can see that the allocated radar energy for each direction is proportional to the interference from the relay communication. Furthermore, in the simulation, the SINR at the radar receiver is 13.8 dB for all detection directions, i.e., $\text{SINR}_k^r = 13.8$ dB, $\forall k$. It is because that we aim to maximize the minimum SINR among all directions, and the maximum value occurs when all SINRs are equivalent.

TABLE I
RUNNING TIME COMPARISON.

The time slot length, L	4	6	8	10	12	14
The CVX solver (s)	0.3425	0.3671	0.4520	0.5845	0.6637	0.7357
The proposed algorithm (s)	0.0377	0.0380	0.0412	0.0487	0.0620	0.0681

TABLE II
MINIMUM RADAR ENERGY COMPARISON.

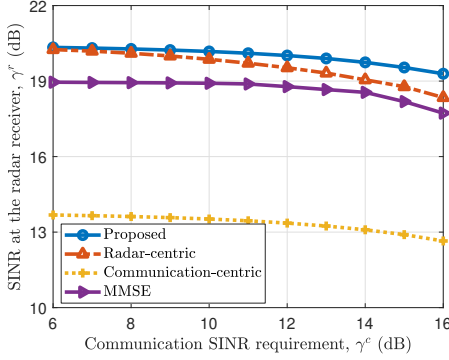| The time slot length, L	4	6	8	10	12	14
The CVX solver (J)	0.0118	0.0363	0.0760	0.2126	0.2384	0.3091
The proposed algorithm (J)	0.0118	0.0363	0.0760	0.2127	0.2385	0.3093

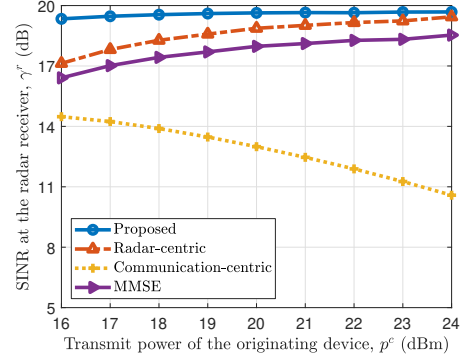Fig. 6. The SINR at the radar receiver vs. the communication SINR requirement.

Fig. 7. The SINR at the radar receiver vs. the transmit power of the originating device.

C. Performance Comparison

To verify the effectiveness of the proposed algorithm, we compare it with the following benchmark algorithms.

- *Radar-centric algorithm* [5]. The filter vector $\boldsymbol{u_k}$ and transmit power p_k^r for the radar are obtained by solving the radar-energy minimization problem. The relay beamforming matrix $\boldsymbol{W}_k$ is obtained without the consideration of interference from the radar, that is, p_k^r is set as zero in problem (21).
- *Communication-centric algorithm* [5]. We adopt the zero-forcing (ZF) filter for the radar receiver without the consideration of interference from the destination device and the transmit power p_k^r is minimized to meet constraint (19b). The relay beamforming matrix $\boldsymbol{W}_k$ is obtained via solving the relay-energy minimization problem.
- *MMSE algorithm* [48]. The minimum mean-squared-error (MMSE) transceiver design is adopted.

Fig. 6 shows the SINR at the radar receiver versus the communication SINR requirement. Firstly, it is readily seen that our proposed algorithm provides the best SINR performance at the radar receiver among all algorithms. Secondly, the SINR at the radar receiver decreases with the communication SINR requirement since more energy is allocated to the relay to meet the communication requirement. Particularly, the performance gap between the proposed algorithm and the radar-centric algorithm (or the MMSE algorithm) also increases with the communication SINR requirement. It is because that when the communication SINR requirement is low, the energy allocated to the relay is small, and thus, the impact of optimized design on beamforming is also low. As the value of the communication

requirement increases, more energy should be allocated to the relay, thus increasing the performance gap. Thirdly, the radar-centric algorithm shows the best performance and the MMSE algorithm shows the second best performance among the three benchmark algorithms. The reason is that we aim to maximize the radar performance in this paper. The radar-centric algorithm gives the optimal radar transceiver design, and the MMSE algorithm gives the suboptimal radar transceiver design.

Fig. 7 shows the SINR at the radar versus the transmit power of the originating device. From the figure, as the transmit power increases, the SINRs at the radar receiver of the proposed, radar-centric, and MMSE algorithms increase while that of the relay-centric algorithm decreases. The reason can be explained as follows. There are two effects caused by the increase of transmit power on the originating device: 1) the communication SINR requirement is easier to be met and more energy remains; 2) the interference power of the radar increases according to (15). For the proposed, radar-centric, and MMSE algorithms, the second effect can be effectively mitigated by properly designing the receive filter, and thus, the SINR increases with the transmit power. On the other hand, the receive filter in the communication-centric algorithm is not optimal. When the transmit power of the originating device increases, higher interference will lead to the reduction of the SINR.

Fig. 8 depicts the SINR at the radar receiver versus the average power limitation. It can be observed that the SINR increases with the average power limitation in all algorithms since more energy can be allocated to the radar and relay for dual function. Moreover, an upper bound for SINR can be seen since the power of the desired signal
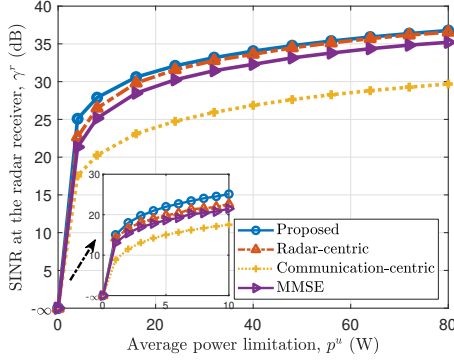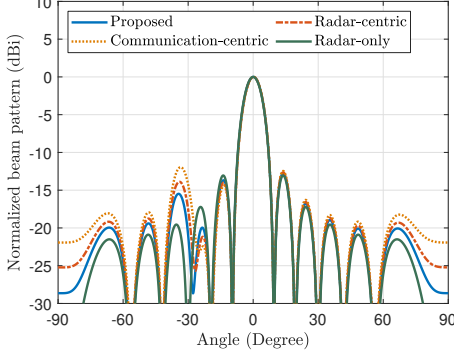
Fig. 8. The SINR at the radar receiver vs. the average power limitation.

Fig. 9. Normalized beam pattern of the dual-functional transmit signal when detection direction is $0°$ and AoAs of channel vector $\boldsymbol{g}$ are $-78°$, $-67°$, $-51°$, and $-38°$.
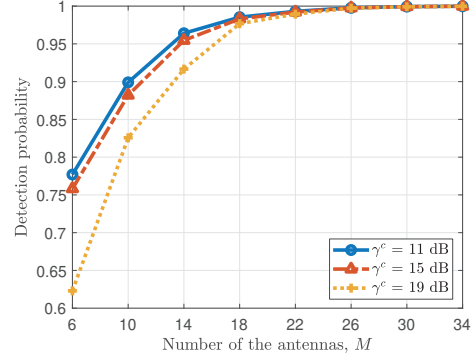

Fig. 10. The minimum detection probability among all directions vs. the number of antennas.

Fig. 11. The ROC curves under different number of antennas.

and interference linearly increases with the energy according to (15). Nevertheless, our proposed algorithm provides the best performance with the lowest average power limitation among all algorithms, which further verifies its effectiveness.

The normalized beam patterns of the dual-functional transmit signal (including both radar and relay) for three algorithms are shown in Fig. 9 when the detection direction is $0°$. Moreover, we also plot the normalized beam pattern of the probing pulse of radar, labeled with "radar-only", for comparison. It is seen that the main lobes of the four beam patterns are almost the same. This guarantees that the dual-functional transmit signal of three algorithms can be utilized for detecting the target along the detection direction. Moreover, it can be observed that the side lobes of four beam patterns are different since the dual-functional transmit signal also contains the relay communication signal. Specifically, the dual-functional transmit signal of the proposed algorithm has a lower side lobe than those of the radar-centric and communication-centric algorithms. We should note that the communication QoS constraint is also satisfied. This verifies that the proposed joint transceiver design algorithm can achieve a high SINR at the radar receiver under the communication constraint.

D. Detection Probability

Fig. 10 shows the minimum detection probability among all directions versus the number of antennas under different communication requirements for the proposed algorithm when the probability of false alarm is 10^{-4}. We can see

that the detection probability increases with the number of antennas since interference from relay communication can be effectively reduced with more antennas. Besides, the detection probability decreases with the communication requirement since less energy should be allocated to the radar under a higher SINR requirement. Meanwhile, we also plot the receiver-operating-characteristic (ROC) curves under different numbers of antennas, as shown in Fig. 11. From the figure, the detection probability increases with the probability of false alarm since it is easier to judge whether there is a target under a higher probability of false alarm. Moreover, when the number of antennas is 30, the detection probability is almost one, which means that the radar signal can be fully separated from the total received signal.

VI. CONCLUSION

In this paper, we have studied the dual-functional FD relay aided radar-communication system, where the coexisted phased-array radar and relay communication share antenna array and spectrum. The minimum SINR at the radar receiver among all detection directions is maximized under the communication QoS requirement and total energy limitation. A mathematical problem has been formulated and further decomposed into the radar-energy and relay-energy minimization problems for each detection direction. For the former, we equivalently transformed it into a convex one and proposed a low-complexity ADMM-based algorithm. For the latter, by introducing an insightful unitary matrix, we simplified it into a QP problem and derived the closed-form expression for the relay beamforming matrix. After that, we

introduced the overall joint transceiver design algorithm and discussed its computational complexity and optimality. Finally, numerical results showed that our proposed algorithm significantly outperforms the benchmark designs.

For simplicity, we only considered one communication pair of transmitter and receiver to gain some insightful results. In the general scenario, there may be multiple communication pairs of transmitter and receiver. When the frequency division multiple access (FDMA) method or time division multiple access (TDMA) method is adopted for the multi-user scenario, our proposed algorithm can be easily extended. Besides, when the space division multiple access (SDMA) method is adopted, the joint transceiver design is much more complicated, which remains an open problem for our future work.

APPENDIX A
PROOF OF THEOREM 1

To prove Theorem 1, we first establish the following lemma.

Lemma 5: The optimal objective value of problem (21) increases as p_k^r increases.

Proof: First, we can rewrite constraint (19c) as

$$\frac{Lp^c \left|\boldsymbol{g}^H \boldsymbol{W}_k \boldsymbol{h}\right|^2 - \gamma^c \left(L\sigma^2 \left|\left|\boldsymbol{g}^H \boldsymbol{W}_k\right|\right|^2 + L\sigma^2\right)}{\gamma^c \left|\boldsymbol{g}^H \boldsymbol{a}^*(\theta_k)\right|^2 + \gamma^c \boldsymbol{g}^H \boldsymbol{W}_k \boldsymbol{P}_k \boldsymbol{W}_k^H \boldsymbol{g}} \geq p_k^r. \quad (39)$$

It is easy to see that the constraint (19c) becomes tighter as p_k^r increases. Meanwhile, constraint (19d) is independent with p_k^r. Thus, we can conclude that the feasible set of problem (21) becomes smaller as p_k^r increases. Moreover, the objective function value of problem (21) increases with p_k^r and the objective function is minimized in problem (21). Therefore, the optimal objective value of problem (21) increases with p_k^r, which ends the proof. ∎

Then, we can prove Theorem 1 as follows. Let $\left\{\boldsymbol{u}_k^+, p_k^{r,+}, \boldsymbol{W}_k^+\right\}$ denote the optimal solution to problem (19) and O^+ represent the corresponding optimal objective value. Let $O^\star$ denote the objective value when the solution is $\left\{\boldsymbol{u}_k^\star, p_k^{r,\star}, \boldsymbol{W}_k^\star\right\}$. First, we prove that $\left\{\boldsymbol{u}_k^\star, p_k^{r,\star}, \boldsymbol{W}_k^\star\right\}$ is a feasible solution to problem (19) as follows. Since $\left\{\boldsymbol{u}_k^\star, p_k^{r,\star}\right\}$ is the solution to problem (20), constraint (19b) is satisfied. Meanwhile, $\boldsymbol{W}_k^\star$ is the solution of problem (21) when $p_k^r = p_k^{r,\star}$, which means that $\left\{p_k^{r,\star}, \boldsymbol{W}_k^\star\right\}$ satisfies constraints (19c) and (19d). Therefore, $\left\{\boldsymbol{u}_k^\star, p_k^{r,\star}, \boldsymbol{W}_k^\star\right\}$ is a feasible solution to problem (19) and we have $O^\star \geq O^+$.

Next, we need to prove $O^\star = O^+$. Since we minimize p_k^r in problem (20) only with constraint (19b), $p_k^{r,\star}$ is no more than $p_k^{r,+}$. Furthermore, $p_k^{r,\star}$ is the tight lower bound of p_k^r in problem (19) since constraint (19b) cannot be satisfied if p_k^r is lower than $p_k^{r,\star}$. Meanwhile, we should note that the optimal value is O^+ when $p_k^r = p_k^{r,+}$ since problem (21) is equivalent to problem (19) when p_k^r is given Thus, based on Lemma 5, we can conclude that $O^\star \leq O^+$ since $p_k^{r,\star} \leq p_k^{r,+}$. Combining with $O^\star \geq O^+$, we have $O^\star = O^+$, which ends the proof.

APPENDIX B
PROOF OF LEMMA 2

Let $\boldsymbol{u}_k^\star$ denote the optimal solution to problem (20). Then, we can find that $a\boldsymbol{u}_k^\star$ is also the optimal solution for any $a \in \mathbb{C}$. Therefore, we can add a constraint into problem (20) without changing the optimal value, that is, $\boldsymbol{u}_k^H \boldsymbol{a}(\theta_k) = 1$. After that, constraint (19b) can be rewritten as

$$\left|\boldsymbol{u}_k^H \boldsymbol{A}_k[l] \boldsymbol{a}^*(\theta_k)\right|^2 + \frac{p^c \left|\boldsymbol{u}_k^H \boldsymbol{h}\right|^2 + \sigma^2 \left|\left|\boldsymbol{u}_k\right|\right|^2}{p_k^r}$$

$$= \left|\boldsymbol{u}_k^H \boldsymbol{A}_k[l] \boldsymbol{a}^*(\theta_k)\right|^2 + \chi_k \leq \frac{\left|\alpha_k[l]\right|^2}{\gamma^r}, \ \forall l \in \mathbb{L}. \quad (40)$$

Then, problem (20) is equivalently transformed into problem (22).

We then prove that problem (22) is convex. It is easy to find that constraints (22b) and (22c) are convex. For the objective function (22a), the Hessian matrix is

$$\boldsymbol{H} = 2 \begin{bmatrix} \dfrac{p^c \boldsymbol{h}\boldsymbol{h}^H + \sigma^2 \boldsymbol{I}}{\chi_k} & -\dfrac{p^c \boldsymbol{h}\boldsymbol{h}^H \boldsymbol{u}_k + \sigma^2 \boldsymbol{u}_k}{\chi_k^2} \\ -\dfrac{p^c \boldsymbol{u}_k^H \boldsymbol{h}\boldsymbol{h}^H + \sigma^2 \boldsymbol{u}_k^H}{\chi_k^2} & \dfrac{p^c \boldsymbol{u}_k^H \boldsymbol{h}\boldsymbol{h}^H \boldsymbol{u}_k + \sigma^2 \boldsymbol{u}_k^H \boldsymbol{u}_k}{\chi_k^3} \end{bmatrix} \quad (41)$$

For any vector $[\boldsymbol{z}^H \ z_{M+1}]^H \in \mathbb{C}^{(M+1)\times 1}$, we have

$$\begin{bmatrix} \boldsymbol{z}^H & z_{M+1}^* \end{bmatrix} \boldsymbol{H} \begin{bmatrix} \boldsymbol{z} \\ z_{M+1}^* \end{bmatrix}$$

$$= \frac{2 \left|\left| \left(p^c \boldsymbol{h}\boldsymbol{h}^H + \sigma^2 \boldsymbol{I}\right)^{1/2} \left(\chi_k \boldsymbol{z} - z_{M+1} \boldsymbol{u}_k\right) \right|\right|^2}{\chi_k^3} \geq 0. \quad (42)$$

Therefore, the objective function is convex. To sum up, problem (22) is convex.

APPENDIX C
DETAILS OF PROPOSED ADMM-BASED ALGORITHM

In this appendix, we show the detailed derivation of solving problems (27) and (28) in the ADMM-based algorithm.

A. Optimal Solution to Problem (27)

The Lagrange function of problem (27) can be defined as

$$\mathcal{L}(\mathbb{Z}_1, \vartheta) = \mathcal{L}_\rho(\mathbb{Z}_1, \mathbb{Z}_2; \boldsymbol{\lambda}_{k,l}, \nu_{k,l}) + \vartheta\left(\boldsymbol{u}_k^H \boldsymbol{a}(\theta_k) - 1\right), \quad (43)$$

where ϑ is the Lagrange multiplier for constraint (22b). Then, by checking the necessary and sufficient conditions based on the KKT conditions, the optimal solution can be expressed as

$$\vartheta^\star = \frac{\boldsymbol{a}^H(\theta_k)\left((L-1)\rho\boldsymbol{I} + \frac{2\boldsymbol{C}}{\chi_k^\star}\right)^{-1}\rho\sum\limits_{l\in\mathbb{L}}\left(\widehat{\boldsymbol{u}}_{k,l} - \frac{\boldsymbol{\lambda}_{k,l}}{\rho}\right) - 1}{\boldsymbol{a}^H(\theta_k)\left((L-1)\rho\boldsymbol{I} + \frac{2\boldsymbol{C}}{\chi_k^\star}\right)^{-1}\boldsymbol{a}(\theta_k)}, \quad (44)$$

$$\boldsymbol{u}_k^\star = \left((L-1)\rho\boldsymbol{I} + \frac{2\boldsymbol{C}}{\chi_k^\star}\right)^{-1}$$
$$\times \left(\rho\sum\limits_{l\in\mathbb{L}}\left(\widehat{\boldsymbol{u}}_{k,l} - \frac{\boldsymbol{\lambda}_{k,l}}{\rho}\right) - \vartheta^\star \boldsymbol{a}(\theta_k)\right), \quad (45)$$

where $\boldsymbol{C} \triangleq p^c \boldsymbol{h}\boldsymbol{h}^H + \sigma^2 \boldsymbol{I}$ and $\chi_k^\star$ is the optimal value satisfying the first-order optimality condition, as

$$\rho \sum_{l \in \mathbb{L}} (\chi_k^\star - \widehat{\chi}_{k,l} + \nu_{k,l}/\rho) - \frac{\boldsymbol{u}^{H,\star} \boldsymbol{C} \boldsymbol{u}^\star}{(\chi_k^\star)^2} = 0. \qquad (46)$$

Note that $\left((L-1)\rho\boldsymbol{I} + \frac{2\boldsymbol{C}}{\chi_k^\star}\right)^{-1} = \left((L-1)\rho + \frac{\sigma^2}{\chi_k^\star}\right)^{-1} \boldsymbol{I}$

$-\frac{\left((L-1) + \rho\frac{\sigma^2}{\chi_k^\star}\right)^{-1} \boldsymbol{h}\boldsymbol{h}^H}{\chi_k^\star(L-1)\rho + \sigma^2 + \boldsymbol{h}^H\boldsymbol{h}}$, which can reduce the computation complexity. Then, By performing the bisection search until equation (46) is satisfied, the optimal solution to problem (27) can be obtained.

B. Optimal Solution to Problem (28)

Problem (28) can be decomposed into several subproblems over each time index $l \in \mathbb{L}$, as,

$$\min_{\{\widehat{\boldsymbol{u}}_{k,l}, \widehat{\chi}_{k,l}\}} \quad \frac{\rho}{2} \left\| \boldsymbol{u}_k - \widehat{\boldsymbol{u}}_{k,l} + \frac{1}{\rho}\boldsymbol{\lambda}_{k,l} \right\|^2$$

$$+ \frac{\rho}{2} \left\| \chi_k - \widehat{\chi}_{k,l} + \frac{1}{\rho}\nu_{k,l} \right\|^2, \qquad (47a)$$

$$\text{s.t.} \qquad \left| \widehat{\boldsymbol{u}}_{k,l}^H \boldsymbol{A}_k[l]\boldsymbol{a}^*(\theta_k) \right|^2 + \widehat{\chi}_{k,l} \leq \frac{\|\alpha_k[l]\|^2}{\gamma^r}. \qquad (47b)$$

Similar to problem (28), we can obtain the following optimal solution

$$\widehat{\chi}_{k,l}^\star = \left(\chi_k + \frac{1}{\rho}\nu_{k,l} - \frac{1}{\rho}\psi^\star \right)^+, \qquad (48)$$

$$\widehat{\boldsymbol{u}}_{k,l}^\star = \boldsymbol{U}_k[l] \left(\rho\boldsymbol{I} + 2\psi^\star\Sigma_k[l] \right)^{-1} \boldsymbol{U}_k^H[l]\rho \left(\boldsymbol{u}_k + \frac{\boldsymbol{\lambda}_{k,l}}{\rho} \right), \qquad (49)$$

where $(x)^+ = \max\{x, 0\}$, $\psi^\star$ is the optimal Lagrange multiplier for constraint (47b), and $\boldsymbol{U}_k[l]\Sigma_k[l]\boldsymbol{U}_k^H[l]$ is the singular value decomposition (SVD) of $\boldsymbol{A}_k[l]\boldsymbol{A}_k^H[l]$. Note that $\Sigma_k[l]$ is a diagonal matrix and m-th diagonal element is $\sigma_{k,m}[l]$. Moreover, $\psi^\star$ should satisfy the complementary slackness condition, as

$$\left(\left(\sum_{m=1}^M (2\psi^\star\sigma_{k,m}[l] + 1)^{-1}(\rho\boldsymbol{u}_k + \boldsymbol{\lambda}_{k,l})^H \boldsymbol{A}_k[l]\boldsymbol{a}^*(\theta_k) \right)^2 \right.$$

$$\left. + \widehat{\chi}_{k,l}^\star - \frac{\|\alpha_k[l]\|^2}{\gamma^r} \right) \psi^\star = 0. \qquad (50)$$

By performing the bisection search until equation (50) is satisfied, the optimal solution to problem (28) can be obtained.

APPENDIX D
PROOF OF THEOREM 2

First, we rewrite $\boldsymbol{z}_{k,m}$ as the linear combination of $\boldsymbol{Q}_k^H\boldsymbol{g}$ and a residual vector, denoted by $\boldsymbol{r}_{k,m}$, that is

$$\boldsymbol{z}_{k,m} = \beta_{k,m}\boldsymbol{Q}_k^H\boldsymbol{g} + \boldsymbol{r}_{k,m}, \forall m, \qquad (51)$$

where $\boldsymbol{r}_{k,m}^H \boldsymbol{Q}_k^H \boldsymbol{g} = 0$. Then, problem (32) becomes

$$\min_{\{\beta_{k,m}, \boldsymbol{r}_{k,m}\}} \left\| \boldsymbol{Q}_k^H\boldsymbol{g} \right\|^2 \left(\sum_{i=1}^M \sum_{j=1}^M \boldsymbol{q}_{k,i}^H \boldsymbol{P}_k \boldsymbol{q}_{k,j} \beta_{k,j}^* \beta_{k,i} \right.$$

$$+ Lp^c \|\boldsymbol{h}\|^2 |\beta_{k,1}|^2 + L\sigma^2 \sum_{m=1}^M |\beta_{k,m}|^2 \Bigg)$$

$$+ Lp^c \|\boldsymbol{h}\|^2 \boldsymbol{r}_{k,1}^H \boldsymbol{r}_{k,1} + L\sigma^2 \sum_{m=1}^M \|\boldsymbol{r}_{k,m}\|^2$$

$$+ \sum_{i=1}^M \sum_{j=1}^M \boldsymbol{q}_{k,i}^H \boldsymbol{P}_k \boldsymbol{q}_{k,j} \boldsymbol{r}_{k,j}^H \boldsymbol{r}_{k,i}, \qquad (52a)$$

$$\text{s.t.} \quad \gamma^c \left(\left| \boldsymbol{g}^H \boldsymbol{v}_k \right|^2 + L\sigma^2 \left\| \boldsymbol{Q}_k^H\boldsymbol{g} \right\|^4 \sum_{m=1}^M |\beta_{k,m}|^2 \right.$$

$$+ \left\| \boldsymbol{Q}_k^H\boldsymbol{g} \right\|^4 \sum_{i=1}^M \sum_{j=1}^M \boldsymbol{q}_{k,i}^H \boldsymbol{P}_k \boldsymbol{q}_{k,j} \beta_{k,j}^* \beta_{k,i}$$

$$+ L\sigma^2 \Bigg) \leq Lp^c \|\boldsymbol{h}\|^2 \left\| \boldsymbol{Q}_k^H\boldsymbol{g} \right\|^4 |\beta_{k,1}|^2, \quad (52b)$$

$$\boldsymbol{q}_{k,2}^H \boldsymbol{a}(\theta_k)\beta_{k,2} + \boldsymbol{q}_{k,1}^H \boldsymbol{a}(\theta_k)\beta_{k,1} = 0, \qquad (52c)$$

$$\boldsymbol{q}_{k,2}^H \boldsymbol{a}(\theta_k)\boldsymbol{r}_{k,2} + \boldsymbol{q}_{k,1}^H \boldsymbol{a}(\theta_k)\boldsymbol{r}_{k,1} = 0. \qquad (52d)$$

By observing this problem, it is easy to find that $\boldsymbol{r}_{k,m}$ should be $\boldsymbol{0}$ when $\boldsymbol{z}_{k,m}$ achieves the optimal solution.

APPENDIX E
PROOF OF LEMMA 3

First of all, we note that $\eta_{k,1} = 1$ and $\eta_{k,2} = -\dfrac{\boldsymbol{q}_{k,1}^H \boldsymbol{a}(\theta_k)}{\boldsymbol{q}_{k,2}^H \boldsymbol{a}(\theta_k)}$ for satisfying constraint (35c). Moreover, constraint (35b) can be rewritten as (54). The equality in (53) holds when the right-hand side of (54) is greater than zero since $\beta_{k,1}$ is independent with $\eta_{k,m}$. We should note that there is no feasible solution if the right hand of (54) is less than zero. Then, the objective function (35a) can be represented as (56). Similar to the above, the equality in (56) also holds. Therefore, minimizing E_k^c is equivalent to minimizing the right-hand side of inequation (56). Furthermore, by analyzing the right-hand side of inequation (56), we can find that it is also identical to minimizing $L\sigma^2 \sum_{m=1}^M |\eta_{k,m}|^2 + p_k^r \sum_{i=1}^M \sum_{j=1}^M \boldsymbol{q}_{k,i}^H \boldsymbol{P}_k \boldsymbol{q}_{k,j} \eta_{k,j}^* \eta_{k,i}$ with $\eta_{k,1} = 1$ and $\eta_{k,2} = -\dfrac{\boldsymbol{q}_{k,1}^H \boldsymbol{a}(\theta_k)}{\boldsymbol{q}_{k,2}^H \boldsymbol{a}(\theta_k)}$. This completes the proof.

APPENDIX F
PROOF OF THEOREM 3

The Lagrange function of the problem (35) can be defined as

$$\mathcal{L} = L\sigma^2 \sum_{m=1}^M |\eta_{k,m}|^2 + p_k^r \sum_{i=1}^M \sum_{j=1}^M \boldsymbol{q}_{k,i}^H \boldsymbol{P}_k \boldsymbol{q}_{k,j} \eta_{k,j}^* \eta_{k,i}. \quad (57)$$

$$|\beta_{k,1}|^2 \geq \frac{\left(p_k^r \left|\boldsymbol{g}^H \boldsymbol{a}^*(\theta_k)\right|^2 + L\sigma^2\right) / \left(\left\|\boldsymbol{Q}_k^H \boldsymbol{g}\right\|^4\right)}{\frac{Lp^c \left\|\boldsymbol{h}\right\|^2}{\gamma^c} - p_k^r \sum_{i=1}^{M} \sum_{j=1}^{M} \boldsymbol{q}_{k,i}^H \boldsymbol{P}_k \boldsymbol{q}_{k,j} \frac{\beta_{k,j}^* \beta_{k,i}}{|\beta_{k,1}|^2} - L\sigma^2 \sum_m \frac{|\beta_{k,m}|^2}{|\beta_{k,1}|^2}} \tag{53}$$

$$= \frac{\left(p_k^r \left|\boldsymbol{g}^H \boldsymbol{a}^*(\theta_k)\right|^2 + L\sigma^2\right) / \left(\left\|\boldsymbol{Q}_k^H \boldsymbol{g}\right\|^4\right)}{\frac{Lp^c \left\|\boldsymbol{h}\right\|^2}{\gamma^c} - p_k^r \sum_{i=1}^{M} \sum_{j=1}^{M} \boldsymbol{q}_{k,i}^H \boldsymbol{P}_k \boldsymbol{q}_{k,j} \eta_{k,j}^* \eta_{k,i} - L\sigma^2 \sum_{m=1}^{M} |\eta_{k,m}|^2}. \tag{54}$$

$$E_k^c = \left\|\boldsymbol{Q}_k^H \boldsymbol{g}\right\|^2 |\beta_{k,1}|^2 \left(Lp^c \left\|\boldsymbol{h}\right\|^2 + L\sigma^2 \sum_{m=1}^{M} |\eta_{k,m}|^2 + p_k^r \sum_{i=1}^{M} \sum_{j=1}^{M} \boldsymbol{q}_{k,i}^H \boldsymbol{P}_k \boldsymbol{q}_{k,j} \eta_{k,j}^* \eta_{k,i}\right) \tag{55}$$

$$\geq \frac{p_k^r \left|\boldsymbol{g}^H \boldsymbol{a}^*(\theta_k)\right|^2 + L\sigma^2}{\left\|\boldsymbol{Q}_k^H \boldsymbol{g}\right\|^2} \cdot \frac{Lp^c \left\|\boldsymbol{h}\right\|^2 + L\sigma^2 \sum_{m=1}^{M} |\eta_{k,m}|^2 + p_k^r \sum_{i=1}^{M} \sum_{j=1}^{M} \boldsymbol{q}_{k,i}^H \boldsymbol{P}_k \boldsymbol{q}_{k,j} \eta_{k,j}^* \eta_{k,i}}{\frac{Lp^c \left\|\boldsymbol{h}\right\|^2}{\gamma^c} - p_k^r \sum_{i=1}^{M} \sum_{j=1}^{M} \boldsymbol{q}_{k,i}^H \boldsymbol{P}_k \boldsymbol{q}_{k,j} \eta_{k,j}^* \eta_{k,i} - L\sigma^2 \sum_{m=1}^{M} |\eta_{k,m}|^2}. \tag{56}$$

To achieve the optimal solution, the partial derivative of $\mathcal{L}$ on $\eta_{k,m}$ should equal zero, that is

$$\frac{\partial \mathcal{L}}{\partial \eta_{k,m}^\star} = L\sigma^2 \left(\eta_{k,m}^\star\right)^* + p_k^r \sum_{j=1}^{M} \boldsymbol{q}_{k,i}^H \boldsymbol{P}_k \boldsymbol{q}_{k,j} \left(\eta_{k,j}^\star\right)^*$$
$$= 0, \quad m \in \{3, \cdots, M\}. \tag{58}$$

Therefore, the optimal solution can be shown in equation (37).

APPENDIX G
PROOF OF LEMMA 4

To find the upper bound of the SINR at the radar receiver, we consider a special case that all energy is allocated to the radar and there is no interference. In this case, the SINR at the radar receiver can be simplified as $\gamma^r = \min_k \min_{l \in \mathbb{L}} \left\{ \left(p_k^r |\alpha_k[l]|^2 \left|\boldsymbol{u}_k^H \boldsymbol{a}(\theta_k)\right|^2\right) / \left(\sigma^2 \left\|\boldsymbol{u}_k\right\|^2\right) \right\}$. To improve the SINR, $\boldsymbol{u}_k$ should be aligned with $\boldsymbol{a}(\theta_k)$. Then, $\gamma^r = \min_k \left\{ p_k^r \min_{l \in \mathbb{L}} |\alpha_k[l]|^2 / \sigma^2 \right\} = \min_k \left\{ \frac{p_k^r |\alpha_k|^2}{\sigma^2} \right\}$, where $|\alpha_k| = \min_{l \in \mathbb{L}} |\alpha_k[l]|$. To obtain the upper bound, the energy allocated to the detection direction θ_k is $E_k^r = p_k^r = E^u \left(\sum_{k=1}^{K} |\alpha_k|^{-2}\right) / |\alpha_k|^2$. Therefore, the upper bound is given by $\gamma_{\max}^r = E^u \left(\sum_{k=1}^{K} |\alpha_k|^{-2}\right) / \sigma^2$.

REFERENCES

[1] J. Park, S. Samarakoon, M. Bennis, and M. Debbah, "Wireless network intelligence at the edge," *Proc. IEEE*, vol. 107, no. 11, pp. 2204–2239, Nov. 2019.

[2] W. Saad, M. Bennis, and M. Chen, "A vision of 6G wireless systems: Applications, trends, technologies, and open research problems," *IEEE Netw.*, vol. 34, no. 3, pp. 134–142, May 2020.

[3] A. Bourdoux *et al.*, "6G white paper on localization and sensing," arXiv preprint arXiv:2006.01779, 2020.

[4] G. R. Curry, *Radar System Performance Modeling*. Norwood, MA: Artech House, 2005.

[5] L. Zheng, M. Lops, Y. C. Eldar, and X. Wang, "Radar and communication coexistence: An overview: A review of recent methods," *IEEE Signal Process. Mag.*, vol. 36, no. 5, pp. 85–99, Sep. 2019.

[6] S. Sodagari, A. Khawar, T. C. Clancy, and R. McGwier, "A projection based approach for radar and telecommunication systems coexistence," in *Proc. IEEE Global Commun. Conf. (GLOBECOM)*, Anaheim, CA, USA, Dec. 2012, pp. 5010–5014.

[7] B. Li, A. P. Petropulu, and W. Trappe, "Optimum co-design for spectrum sharing between matrix completion based MIMO radars and a MIMO communication system," *IEEE Trans. Signal Process.*, vol. 64, no. 17, pp. 4562–4575, Sep. 2016.

[8] J. Qian, M. Lops, L. Zheng, X. Wang, and Z. He, "Joint system design for co-existence of MIMO radar and MIMO communication," *IEEE Trans. Signal Process.*, vol. 66, no. 13, pp. 3504–3519, Jul. 2018.

[9] F. Wang, H. Li, and M. A. Govoni, "Power allocation and co-design of multicarrier communication and radar systems for spectral coexistence," *IEEE Trans. Signal Process.*, vol. 67, no. 14, pp. 3818–3831, Jul. 2019.

[10] F. Liu, C. Masouros, A. Li, T. Ratnarajah, and J. Zhou, "MIMO radar and cellular coexistence: A power-efficient approach enabled by interference exploitation," *IEEE Trans. Signal Process.*, vol. 66, no. 14, pp. 3681–3695, Jul. 2018.

[11] F. Liu, C. Masouros, A. Li, and T. Ratnarajah, "Robust MIMO beamforming for cellular and radar coexistence," *IEEE Wireless Commun. Lett.*, vol. 6, no. 3, pp. 374–377, Jun. 2017.

[12] F. Wang and H. Li, "Joint waveform and receiver design for cochannel hybrid active-passive sensing with timing uncertainty", *IEEE Trans. Signal Process.*, vol. 68, pp. 466–477, Jan. 2020.

[13] A. Hassanien, M. G. Amin, E. Aboutanios, and B. Himed, "Dual-function radar communication systems: A solution to the spectrum congestion problem," *IEEE Signal Process. Mag.*, vol. 36, no. 5, pp. 115–126, Sep. 2019.

[14] A. R. Chiriyath, B. Paul, and D. W. Bliss, "Radar-communications convergence: Coexistence, cooperation, and co-design," *IEEE Trans. Cogn. Commun. Netw.*, vol. 3, no. 1, pp. 1–12, Mar. 2017.

[15] F. Liu, C. Masouros, A. Li, H. Sun, and L. Hanzo, "MU-MIMO communications with MIMO radar: From co-existence to joint transmission," *IEEE Trans. Wireless Commun.*, vol. 17, no. 4, pp. 2755–2770, Apr. 2018.

[16] F. Liu, L. Zhou, C. Masouros, A. Li, W. Luo, and A. Petropulu, "Toward dual-functional radar-communication systems: Optimal waveform design," *IEEE Trans. Signal Process.*, vol. 66, no. 16, pp. 4264–4279, Aug. 2018.

[17] Y. Zhao, Y. Chen, M. Ritchie, W. Su, and H. Gu, "MIMO dual-

functional radar-communication waveform design with peak average power ratio constraint," *IEEE Access*, vol. 9, pp. 8047–8053, Jan. 2021.

[18] F. Liu, C. Masouros, A. P. Petropulu, H. Griffiths, and L. Hanzo, "Joint radar and communication design: Applications state-of-the-art and the road ahead," *IEEE Trans. Commun.*, vol. 68, no. 6, pp. 3834–3862, Jun. 2020.

[19] Y. Yang, H. Hu, J. Xu, and G. Mao, "Relay technologies for WiMAX and LTE-advanced mobile systems," *IEEE Commun. Mag.*, vol. 47, no. 10, pp. 100–105, Oct. 2009.

[20] L. Sanguinetti, A. A. DAmico, and Y. Rong, "A tutorial on the optimization of amplify-and-forward MIMO relay systems," *IEEE J. Sel. Areas Commun.*, vol. 30, no. 8, pp. 1331–1346, Sep. 2012.

[21] Y. Cai, Q. Shi, B. Champagne, and G. Y. Li, "Joint transceiver design for secure downlink communications over an amplify-and-forward MIMO relay," *IEEE Trans. Comm.*, vol. 65, no. 9, pp. 3691–3704, Sep. 2017.

[22] L. Gerdes, C. Hellings, L. Weiland, and W. Utschick, "On the maximum achievable partial decode-and-forward rate for the Gaussian MIMO relay channel," *IEEE Trans. Inf. Theory*, vol. 61, no. 12, pp. 6751–6758, Dec. 2015.

[23] H. Suraweera, I. Krikidis, G. Zheng, C. Yuen, and P. Smith, "Low-complexity end-to-end performance optimization in MIMO full-duplex relay," *IEEE Trans. Wireless Commun.*, vol. 13, no. 2, pp. 913–927, Feb. 2014.

[24] O. Taghizadeh, J. Zhang, and M. Haardt, "Transmit beamforming aided amplify-and-forward MIMO full-duplex relaying with limited dynamic range," *Signal Process.*, vol. 127, pp. 266–281, Oct. 2016.

[25] Q. Shi, M. Hong, X. Gao, E. Song, Y. Cai, and W. Xu, "Joint source-relay design for full-duplex MIMO AF relay systems," *IEEE Trans. Signal Process.*, vol. 64, no. 23, pp. 6118–6131, Dec. 2016.

[26] Y. Cai, Y. Xu, Q. Shi, B. Champagne and L. Hanzo, "Robust joint hybrid transceiver design for millimeter wave full-duplex MIMO relay systems," *IEEE Trans. Wireless Commun.*, vol. 18, no. 2, pp. 1199–1215, Feb. 2019.

[27] L. Zhu, J. Zhang, Z. Xiao, X. Cao, X.-G. Xia, and R. Schober, Millimeter-wave full-duplex UAV relay: Joint positioning, beamforming, and power control, *IEEE J. Sel. Areas Commun.*, vol. 38, no. 9, pp. 2057–2073, Sep. 2020.

[28] F. Liu, Y. Cui, C. Masouros, J. Xu, T. X. Han, Y. C. Eldar, and S. Buzzi, "Integrated sensing and communications: Toward dual-functional wireless networks for 6G and beyond," *IEEE J. Sel. Areas Commun.*, vol. 40, no. 6, pp. 1728–1767, Jun. 2022.

[29] F. Bozorgi, P. Sen, A. N. Barreto, and G. Fettweis, "RF Front-End Challenges for Joint Communication and Radar Sensing," in *Proc. 1st IEEE Int. Online Symp. Joint Commun. Sens.*, Feb. 2021, pp. 1–6.

[30] J. A. Zhang, F. Liu, C. Masouros, R. W. Heath, Z. Feng, L. Zheng, and A. Petropulu, "An overview of signal processing techniques for joint communication and radar sensing," 2021, *arXiv:2102.12780*. [Online]. Available: https://arxiv.org/abs/2102.12780

[31] M. A. Richards, J. A. Scheer, and W. A. Holm, *Principles of Modern Radar: Basic Principles*. New York, NY, USA: Scitech, 2010.

[32] K. F. Hasan, Y. Feng, and Y.-C. Tian, "GNSS time synchronization in vehicular ad-hoc networks: Benefits and feasibility," *IEEE Trans. Intell. Transport. Syst.*, vol. 19, no. 12, pp. 3915–3924, Dec. 2018.

[33] A. Tang, S. Li, and X. Wang, "Self-interference-resistant IEEE 802.11ad-based joint communication and automotive radar design," *IEEE J. Sel. Top. Signal Process.*, vol. 15, no. 6, pp. 1484–1499, 2021.

[34] C. Baquero Barneto, T. Riihonen, M. Turunen, L. Anttila, M. Fleischer, K. Stadius, J. Ryyänen, and M. Valkama, "Full-duplex OFDM radar with LTE and 5G NR waveforms: Challenges, solutions, and measurements," *IEEE Trans. Microw. Theory Tech.*, vol. 67, no. 10, pp. 4042–4054, 2019.

[35] C. B. Barneto, S. D. Liyanaarachchi, M. Heino, T. Riihonen, and M. Valkama, "Full duplex radio/radar technology: The enabler for advanced joint communication and sensing," *IEEE Wireless Commun.*, vol. 28, no. 1, pp. 82–88, 2021.

[36] D. Bharadia, E. McMilin, and S. Katti, "Full duplex radios," in *Proc. ACM SIGCOMM*, Aug. 2013, pp. 375–386.

[37] T. Riihonen, S. Werner, and R. Wichman, "Mitigation of loopback self-interference in full-duplex MIMO relays," *IEEE Trans. Signal Process.*, vol. 59, no. 12, pp. 5983–5993, Dec. 2011.

[38] P. Lioliou, M. Viberg, M. Coldrey, and F. Athley, "Self-interference suppression in full-duplex MIMO relays," in *Conf. Rec. 44th Asilomar Signals, Syst. Comput. Conf.*, Pacific Grove, CA, USA, Nov. 2010, pp. 658–662.

[39] W. Yuan, F. Liu, C. Masouros, J. Yuan, D. W. K. Ng, and N. Gonzlez-Prelcic, "Bayesian predictive beamforming for vehicular networks: A low-overhead joint radar-communication approach," *IEEE Trans. Wireless Commun.*, vol. 20, no. 3, pp. 1442–1456, Mar. 2021.

[40] M. Grant and S. Boyd, "CVX: MATLAB software for disciplined convex programming, version 2.1," Mar. 2014. [Online]. Available: http://cvxr.com/cvx.

[41] S. Boyd, "Distributed optimization and statistical learning via the alternating direction method of multipliers," *Found. Trends Mach. Learn.*, vol. 3, no. 1, pp. 1–122, Jan. 2010.

[42] D. P. Bertsekas and J. N. Tsitsiklis, *Parallel and Distributed Computation: Numerical Methods Belmont*, MA, USA: Athena Scientific, 1997.

[43] Q. Hu, Y. Cai, A. Liu, G. Yu, and G. Y. Li, "Low-complexity joint resource allocation and trajectory design for UAV-aided relay networks with the segmented ray-tracing channel model," *IEEE Trans. Wireless Commun.*, vol. 19, no. 9, pp. 6179–6195, Sep. 2020.

[44] K.-Y. Wang, A. M.-C. So, T.-H. Chang, W.-K. Ma, and C.-Y. Chi, "Outage constrained robust transmit optimization for multiuser MISO downlinks: Tractable approximations by conic optimization," *IEEE Trans. Signal Process.*, vol. 62, no. 21, pp. 5690–5705, Nov. 2014.

[45] J. Horn and C. R. Johnson, *Matrix Analysis*. Cambridge Univ. Press, 2013.

[46] S. Boyd and L. Vandenberghe, *Convex Optimization*. Cambridge, U.K.: Cambridge Univ. Press, 2004.

[47] A. Liu, V. K. N. Lau, and M. Zhao, "Stochastic successive convex optimization for two-timescale hybrid precoding in massive MIMO," *IEEE J. Sel. Topics Signal Process.*, vol. 12, no. 3, pp. 432–444, Jun. 2018.

[48] C. T. Lin, F. S. Tseng, and W. R. Wu, "MMSE transceiver design for full-duplex MIMO relay systems," *IEEE Trans. Veh. Technol.*, vol. 66, no. 8, pp. 6849–6861, Aug. 2017.